

Washington University in St. Louis

## Washington University Open Scholarship

---

All Theses and Dissertations (ETDs)

---

1-1-2011

### Design, Construction and Testing of a High Temperature High Pressure Spectroscopic Cell for Polymer Physics Studies

Sai Janani Ganesan

*Washington University in St. Louis*

Follow this and additional works at: <https://openscholarship.wustl.edu/etd>

---

#### Recommended Citation

Ganesan, Sai Janani, "Design, Construction and Testing of a High Temperature High Pressure Spectroscopic Cell for Polymer Physics Studies" (2011). *All Theses and Dissertations (ETDs)*. 503. <https://openscholarship.wustl.edu/etd/503>

This Thesis is brought to you for free and open access by Washington University Open Scholarship. It has been accepted for inclusion in All Theses and Dissertations (ETDs) by an authorized administrator of Washington University Open Scholarship. For more information, please contact [digital@wumail.wustl.edu](mailto:digital@wumail.wustl.edu).

WASHINGTON UNIVERSITY IN ST. LOUIS

School of Engineering and Applied Science

Department of Biomedical Engineering

Thesis Examination Committee:

Carl Frieden, Chair

Rohit Pappu

Donald Elbert

DESIGN, CONSTRUCTION AND TESTING OF HIGH TEMPERATURE- HIGH  
PRESSURE SPECTROSCOPIC CELL FOR POLYMER PHYSICS STUDIES

by

Sai Janani Ganesan

A thesis presented to the School of Engineering  
of Washington University in partial fulfillment of the  
requirements for the degree of

MASTER OF SCIENCE

May 2011  
Saint Louis, Missouri

## ABSTRACT OF THE THESIS

### Design, Construction and Testing of High Temperature-High Pressure Spectroscopic Cell for Polymer Physics Studies by

Sai Janani Ganesan

Master of Science in Biomedical Engineering

Washington University in St. Louis, 2011

Research Advisor: Professor Carl Frieden

Knowledge of phase behaviour of polymer solutions is critical in understanding their chemical and physical properties. Proteins are polymers and aggregation is a phase separation process, hence there is a need for the use of techniques from polymer physics to characterize phase diagrams. Prior work on protein aggregation indicates the need for superheated water to disaggregate the system, accordingly this report proposes a simple, efficient, and reliable instrument for experimentally determining cloud-point curves for binary polymer-solvent systems. Cloud-point measurements are a prominent technique in constructing phase diagrams. A one milliliter optical cell has been designed and constructed, to withstand 200 ° Celsius temperature and 3500 Psi. The cell has been used to successfully reconstruct coexistence curves, and identify critical points for different binary polymer-solvent systems, including part of the cloud point curve for PEG-8000 (Poly-(ethylene glycol)<sub>n</sub>)-water, to validate the use of the device. We also report our initial results using aggregation prone protein samples.

# Acknowledgments

I would like to acknowledge the support of many individuals, who have contributed to this thesis in many ways. First of all I would like to thank Dr. Carl Frieden for his patience, and giving me this opportunity to learn. Scott Crick, for his guidance, words can't describe how much I have learnt from him in these two years. Jim Linders, for the fabrication of the instrument and making me better at CAD. I would also like to thank my committee members, who have reviewed this thesis and helped support the related research.

I would like to dedicate this thesis to my father, for being a source of inspiration in my life. Also, this wouldn't have been possible without the wishes and support of my mother and sister.

Sai Janani Ganesan

*Washington University in St. Louis*

*May 2011*

# Contents

Abstract.....	i
Acknowledgments.....	ii
List of Tables.....	v
List of Figures.....	vi
<b>1 Introduction.....</b>	<b>1</b>
1.1 Cloud-point Determination Methods.....	2
1.2 Coexistence Curves.....	3
1.3 Objective.....	4
1.4 High Pressure Cell.....	5
<b>2 Design and Construction.....</b>	<b>7</b>
2.1 Metal Body.....	7
2.1.1 Thermal Conductivity.....	7
2.1.2 Thermal Expansion.....	9
2.1.3 Chemical Reactivity.....	10
2.2 Optical Element.....	10
2.2.1 Window Material.....	10
2.2.2 Window Size.....	11
2.3 Temperature Sensor.....	12
2.3.1 Types of thermocouples.....	12
2.4 Heat Source.....	13
2.4.1 Type and Size.....	14
2.4.2 Wattage and Watt Density.....	14
2.4.3 Other Specifications.....	14
2.5 Insulation.....	15
2.6 Sealing .....	16
2.7 Construction .....	17
2.7.1 Steps for Construction.....	18
<b>3 Detection and Analysis.....</b>	<b>22</b>
3.1 Image and Intensity Analysis.....	24
3.1.1 Analysis on MATLAB.....	24
3.1.2 Characterizing the Setup.....	27
3.2 Determination of LCST of PEG-8000.....	29
3.3 Studying Protein Aggregation.....	38

<b>4 Discussion and Conclusions</b> .....	44
<b>5 Appendix 1</b> .....	47
<b>References</b> .....	51
<b>Vita</b> .....	53

# List of Tables

Table 2.1:	List of metals and their thermal conductivities.....	8
Table 2.2:	List of metals and their thermal expansion coefficients.....	9
Table 2.3:	List of different types of thermocouples.....	13
Table 3.1:	Absorbance and intensity values of milk.....	27

# List of Figures

Figure 1.1: Phase diagram of a binary system.....	3
Figure 2.1: Transmittance range of Sapphire windows .....	11
Figure 2.2: Cross Sectional view of the Insulation .....	15
Figure 2.3: Cross Section of Clamped windows .....	16
Figure 2.4: Swage lock fitting.....	17
Figure 2.5: Complete view of the alignment .....	19
Figure 2.6: Cross Section (Front View) .....	20
Figure 2.7: Cross Section (Side View) .....	20
Figure 2.8: Isometric View .....	21
Figure 2.9: Image of the device.....	22
Figure 3.1: Block diagram of the arrangement.....	23
Figure 3.2: Image of the setup.....	24
Figure 3.3: Images of the video output.....	26
Figure 3.3: Images of the video output.....	26
Figure 3.4: Absorbance vs. Intensity .....	29
Figure 3.5: Turbidity of heating PEG(8000)-water system.....	31
Figure 3.6: Turbidity of cooling PEG(8000)-water system.....	32
Figure 3.7: Direct video capture(heating). .....	33
Figure 3.8: Direct video capture(cooling).....	34
Figure 3.9: Total Intensity Plot of PEG 50%.....	35
Figure 3.10: Intensity plot(heating) .....	36
Figure 3.11: Intensity plot(cooling) .....	36
Figure 3.12: Phase diagram of PEG-water system .....	37
Figure 3.13: Phase diagram of PEG-water system(reference) .....	38
Figure 3.14: Real time images of Polyglutamine(heating) .....	41
Figure 3.15: Real time images of Polyglutamine(cooling) .....	42
Figure 3.16: Real time images of CsgA(heating) .....	43
Figure 3.17: Real time images of CsgA(cooling) .....	44



# Chapter 1

## Introduction

Understanding phase behaviour of polymer-solvent systems is of importance in the study of synthesis, polymerization, and processing. The dynamics of polymer solutions can affect the solubility and the miscibility of the polymer, resulting in phase separation. Since the early part of last century, efforts have been made to collect equilibrium experimental data for different polymer solutions (*Bae et al., 1991; Zeman et al., 1972; Saeki et al., 1976*), one of the popular methods has been through the construction of cloud point curves. The process of phase separation results in a cloudiness or a turbidity in the mixture, the particular point at which the nature of the solution changes is called the cloud point (a temperature and a concentration value). A plot of the cloud point temperature as a function of concentration leads to the construction of coexistence curves (*Delmas et al., 1966*), or a thermodynamic phase diagram which can also provide useful information on the kinetics of the system.

Proteins are heteropolymers consisting of amino acids as its monomers, and protein aggregation is a process of polymer self association which results in phase separation. Thus there exists commonality in self association and aggregation of intrinsically disordered proteins (IDPs) and other synthetic polymers (*Dobson et al., 2006*). The process of aggregation can be described as the domination of chain-chain interaction over chain-solvent interaction, and the polymer is said to be in a poor solvent (*Rubinstein et al., 2003*). The solvent quality can be manipulated by changing temperature and pressure. Also, prior unpublished data indicate that proteins disaggregate in superheated water. Keeping the above in mind, we have constructed a high pressure-high temperature optical cell, that can be used to vary the solvent quality of the protein-solvent systems with temperature, and hence construct complete phase diagrams of aggregation prone proteins.

Presented in this thesis is the design and construction of a simple and reliable instrument to determine cloud point curves of binary protein/polymer-solvent systems. A CCD camera is used as the detection system to measure the absorbance signal, and the data collected are analyzed in MATLAB. This research focuses on developing an instrument that can be used to study protein-solvent systems and gain insights on the process of aggregation.

Outlined below, is a brief overview of the approach, along with other existing techniques for constructing coexistence curves, and some brief thermodynamics concepts that are essential to understand the motivation behind this research. Also, the objective of this thesis is outlined in greater detail.

## 1.1 Cloud-point Determination Methods

Thermo-optical analysis (TOA) for cloud point measurements was first proposed by *Bae et al.* in 1991, and is currently one of the more precise techniques used to determine cloud points, apart from PICS. There have been other successful attempts at building similar systems (*Saraiva et al., 1993 ; Shokonfi et al., 2007; Svaboda et al., 1999; Cesteros et al., 1994*). TOA involves adding samples to pyrex tubes, and placing them on a heating-cooling stage, which is designed for the observation of the sample behaviour under a microscope, and a photodiode is used for the measurement of luminosity. The advantages of our design over the other experimental techniques are the following:

- a) It is simple, small and a compact device that consists of all the basic elements required to make cloud point measurements and can be used and cleaned very easily.
- b) Inserting sample into the cell is very simple, there is no need for sealing of pyrex tubes or liquid nitrogen.
- c) Multiple different measurements can be made (light scattering, absorbance etc), and MATLAB is used for data analysis. Real time videos can also be recorded for further analysis. Even though our instrument is not sensitive to very high turbidity, and is more appropriate or qualitative analysis; it can be integrated with a laser for small angle

light scattering experiments.

## 1.2 Coexistence Curves

UCST or the upper critical solution temperature is defined as the temperature above which; and LCST is the lower critical solution temperature, and is the temperature below which, all compositions of the mixture are miscible and exist in a single phase (Flory et al., 1954; Sanchez et al., 2000). At both the upper and lower two phase envelope, there are two regions of phase separation-the binodal and the spinodal (the intersection of these two curves being the critical point). Between the binodal and spinodal, there is nucleation and growth phase, which requires exceeding an energy barrier, whereas within the spinodal condition phase separation occurs via a process called spinodal decomposition, which is a downhill process. (Flory et al., 1954 ; Crist et al., 1997; Robenson et al., 2007; Rubenstein et al., 2003). Phase separation is accompanied by a change in turbidity, that can be observed for different compositions to plot a graph similar to the one below.

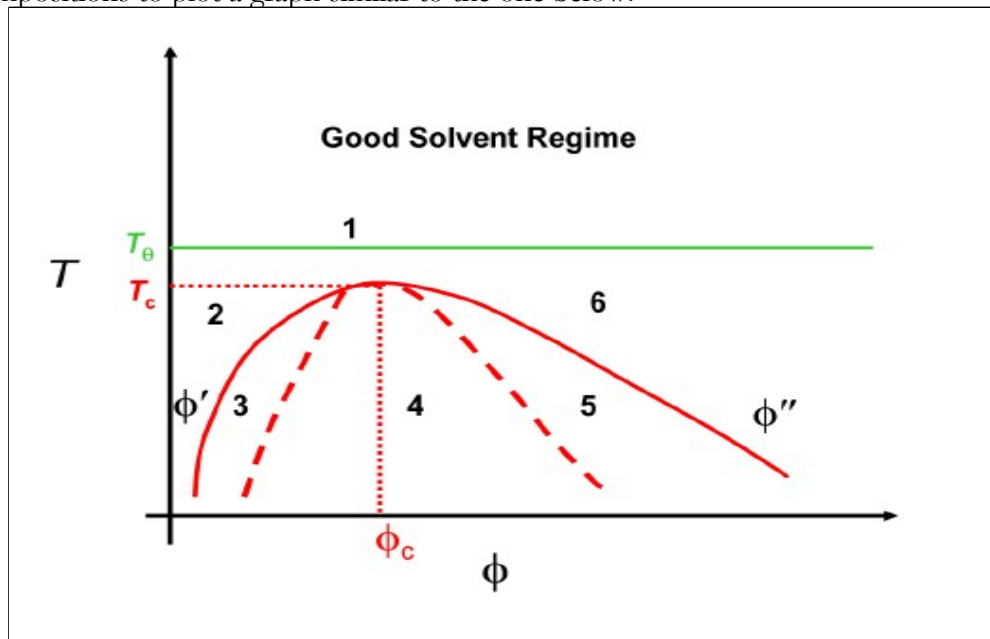


**Figure 1-1. UCST-Phase Diagram of a Binary System.** The plot of temperature vs volume fraction, showing phase separation. The curve defines the boundary of miscibility,  $T_c$  and  $\phi_c$  represents the critical point (Flory et al., 1954; Rubenstein et al., 2003; Pappu et al., 2007).

In the above figure, the temperature controls the solvent quality, and as the temperature is increased, the solvent quality increases till a point is reached, above which the quality of solvent is good for all compositions of the mixture (*Rubinstein et al., 2003; Crick et al., 2010; Flory et al., 1954*).  $\chi$  represents the Flory interaction parameter, and can also be used to characterize the pairwise interaction energies in the binary mixture, which directly affect the solvent quality. With decrease in temperature and hence solvent quality, phase separation into a polymer rich phase and solvent rich phase occurs, and is depicted in the above figure in great detail. Different regions are defined in the above figure to better understand the complete phase diagram.  $T_0$  and  $\varphi_0$  represent the theta temperature or state, at which  $B_2$  or the second virial coefficient goes to zero, and the polymer is in an ideal random coil state and possesses maximum conformational entropy. Beyond the theta temperature, the solvent quality is good for all compositions of the polymer solvent system. Region 1 corresponds to this state. Region 2 represents a region where the mixture is too dilute to undergo any phase transitions. In figure 1.1,  $\varphi'$  and  $\varphi''$  represent the concentration of a dilute polymer solution and a protein aggregated solution respectively. Region 3 represents the region between the binodal and spinodal- the region where there is a requirement for large fluctuations in order to cross the energy barrier and result in phase separation. Region 4 represents the region inside the spinodal, where phase separation occurs by spinodal decomposition.- a process that is thermodynamically downhill and is caused by even the slightest fluctuation in the system. Region 6 is the polymer rich phase (*Rubinstein et al., 2003; Flory et al., 1954*).  $T_c$  and  $\varphi_c$  represent the critical point of the binary mixture, and is the point where the binodal and spinodal intersect, and where fluctuations in conformations are maximum. Chain length plays an important role in characterizing the phase diagram.  $T_c$  decreases with decrease in chain length (*Flory et al., 1954 ; Rubinstein et al., 2003; Crick et al., 2010; Pappu et al. 2007*).

### 1.3 Objective

Investigations have shown how the phase diagram of protein solutions can affect the kinetics and mechanisms of nucleation, and the measurement of cloud-points can provide

details on the attractive forces between the protein molecules (*Galkin et al., 2001; Frenkel et al., 1997*). Prior studies suggest that proteins disaggregate in superheated water, and hence the need for a simple, reliable equipment setup to study protein solutions in high pressure-temperature conditions. Although there have been attempts to construct instruments to determine the cloud points (*Szydlowski et al., 1991*), our instrument is unique in its design and construction, which is based on our needs and constraints. In conclusion, studying temperature induced phase transitions is an effective way to determine the strength of protein interactions (*Lu et al., 2003*), and this instrument will help us gain insight on the process of aggregation.

## 1.4 High Pressure Cell

Phase separation information can be induced by increasing the pressure, temperature among others. Keeping the above concept in mind, a high temperature high pressure cell has been designed, which can be integrated with a laser for small angle scattering experiments. CCD camera is used for detecting absorbance or turbidity, and the results analyzed in MATLAB.

Since there is a need to perform the experiments in superheated water, the optical cell is designed to hold 1 ml of liquid, and tolerate up to 200 °C temperature and 3500 Psi pressure. The above range is again, based on the objective of the experiment, and the initial aim was to construct a cell that can withstand at least 200 °C and the pressure generated at that temperature and then modify the design to achieve higher temperatures and pressures. The cell is fitted with sapphire windows for spectroscopic studies, and two cartridge heaters are fitted equidistant from the center of the cell, as heat sources. The heaters are connected to a power source, and a constant wattage is supplied to the system.

J type thermocouple is used as the temperature sensor, and the gaps are sealed with epoxy. The windows are supported on either sides by aluminum plates to protect against leakage. The detection and analysis is based on measuring absorbance or turbidity with the help of a camera.

A mercury lamp was used as a light source, and a charge couple device-camera to record videos of the light emitted from the optical cell. The videos were analyzed in MATLAB, by converting formatted videos to a series of frames, and then studying the intensity profiles of different frames.

To test the use and performance of the designed optical cell, reconstruction of the cloud point curves, for PEG(Poly-(ethylene glycol)n-8000) -water system was attempted. Similar experiments were performed with polyglutamine, and CsgA-both aggregation prone proteins, to try and observe any phase changes or changes in chain-chain and chain-solvent interactions.

Presented in this thesis is a detailed account of the design and construction of a high temperature high pressure cell, that can operate in superheated water regime also, the use of a detection setup, and the sensitivity of the same in comparison with a spectrophotometer. Initial results with polyglutamine and CsgA are reported as well.

# Chapter 2

## Design and Construction

Design of this device is based on simplicity, optimal utilization of resources and easy workability. Ideal volume of the cell is 1 ml, and the light path is 1 cm, which is critical for spectroscopic applications. The main components of the device include:

- a) Metal body
- b) Optical element
- c) Sensor
- d) Heat source
- e) Insulation
- f) Sealing

### 2.1 Metal Body

The operation range of the device is 25 °C-200 °C, hence the body of the device must be sturdy, have a high thermal conductivity, low thermal expansion, and low reactivity.

#### 2.1.1 Thermal Conductivity

Thermal conductivity,  $k$  is the property of a material to conduct heat. It is commonly defined as, the amount of heat transmitted, over unit temperature gradient, in unit time under steady conditions in a direction normal to a surface of unit area. Based on the value of  $k$ , we evaluate the rate of heat transfer using the below equation:

$$\Delta Q/\Delta t = kA (\Delta T/h) \quad (2.1)$$

Where  $\Delta Q/\Delta t$  is the rate of heat flow,  $k$  is thermal conductivity,  $A$  is total cross sectional area of the surface,  $\Delta T$  is the temperature difference and  $b$  is the thickness of conducting surface. Since the ideal shape of the device is a cylinder, the volume 1 ml, and the optimal range of operation is 25 °C to 200 °C, the above quantities can be easily calculated.

$$H = 1\text{ cm}$$

$$\Pi r^2 h = 1$$

$$r = 0.5643\text{ cm}$$

$$A = 2\Pi r h + 2\Pi r^2 = 5.5435\text{ cm}^2$$

$$\Delta T = 175\text{ (ideal)}$$

From the below table (Table 2.1), it is clear that aluminium and copper were the best options. Copper has more disadvantages, namely; its weight, ability to tarnish quickly and also dissipate heat slower than aluminium. Aluminium, is cheaper and easier to work with and hence was the preferable choice.

Number	Metal	$K$ (W/mK)	$\Delta Q/\Delta t$ (W)
1	Aluminium	250	2425.28
2	C-Steel	54	523.86
3	Iron	80 -60	776.09-582.06
4	Stainless steel	16 -18	155.218-174.62
5	Copper	386	3744.63
6	Invar	10.7	103.8
7	Brass	151	1464.87
8	Kovar	16.3	158.12

**Table 2-1. List of metals and their thermal conductivities.** The above is a list of metals considered for the design, their thermal conductivity and the expected rate of heat flow for the considered design.



## 2.1.2 Thermal Expansion

Matter undergoes a change in volume on heating due to an increase in atomic vibrations which results in an increment in inter atomic distance. The linear thermal expansion coefficient is the measure of change in material length with increasing temperature. It is given by the formula, listed below:

$$\alpha = dl / (l*dT) \quad (2.2)$$

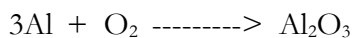
Where  $\alpha$  is the linear thermal expansion coefficient,  $dl$  is the change in length, and  $dT$  is the change in temperature. The change in dimension for a change in temperature of 175 °C, and a thickness of 1 cm is listed in the table below. Increase in temperature can generate detrimental internal stress, which might disturb the sealing and coerce a leakage. From the following table (Table 2.2), it is clear that in the operation range under consideration, the linear expansion of the metal is not going to play a big role. Aluminium was chosen as the metal body for the optical cell.

Number	Metal	$\alpha$ ( $10^{-6}/^{\circ}\text{C}$ )	Change in Length( $dl$ ) in m
1	Aluminium	23	4.03E-005
2	C-steel	10.8	1.89E-005
3	Iron	11.1	1.94E-005
4	Stainless Steel	17.3	3.03E-005
5	Copper	17	2.97E-005
6	Invar	1.2	2.10E-006
7	Brass	19	3.33E-005
8	Sapphire	5.3	9.28E-006

**Table 2-2. List of metals and their thermal expansion coefficient.** The above is a list of metals considered for the design, their thermal expansion coefficient and the expected increase in length for the considered design.

### 2.1.3 Chemical Reactivity

It is critical to consider the reactivity of the metal used, since it is part of the solution chamber and, also will be in direct contact with aqueous solutions. Aluminium is the metal under consideration, and possesses a valency of +3, implying it is relatively unstable vis-a-vis other heat conductive metals, and hence more reactive. However, aluminium has the ability to form an aluminium oxide, in the presence of oxygen, almost instantly. This acts like a protective layer, since the electronegativity of oxygen enables the formation of strong covalent bonds making the layer inert, and stable. Hence the reactivity of the metal is not going to play a big role in any of the experiments.



The above reaction occurs instantaneously, when Al comes in contact with air or water.

## 2.2 Optical Element

Spectroscopic studies of aqueous solutions at high temperature and pressure in the region of superheated water requires optical access, or windows that can withstand the same conditions. The windows must be able to withstand physical stress and chemical corrosion, have a good transmission range, scratch resistant, and easy to handle and seal.

### 2.2.1 Window Material

The purpose of a window is to provide a clear aperture to transmit light. There are many materials that can be used, like BK7 glass, fused silica, quartz etc. Sapphire was chosen as the ideal material due to the following reasons.

- a) It is the best choice for scratch resistant applications due to extreme surface hardness (Mohs=9; Vickers hardness: 2300).
- b) Wider transmission range, most suitable for applications with laser and visible region (figure 2.1).
- c) High thermal conductivity ( $k= 42 \text{ W/(mK)}$ ).
- d) Due to a large structural strength, they can be made much thinner with improved transmittance.
- e) Low thermal expansion, hence the sealing will be easier. ( $\alpha = 5.3 \times 10^{-6}/^\circ\text{C}$ )

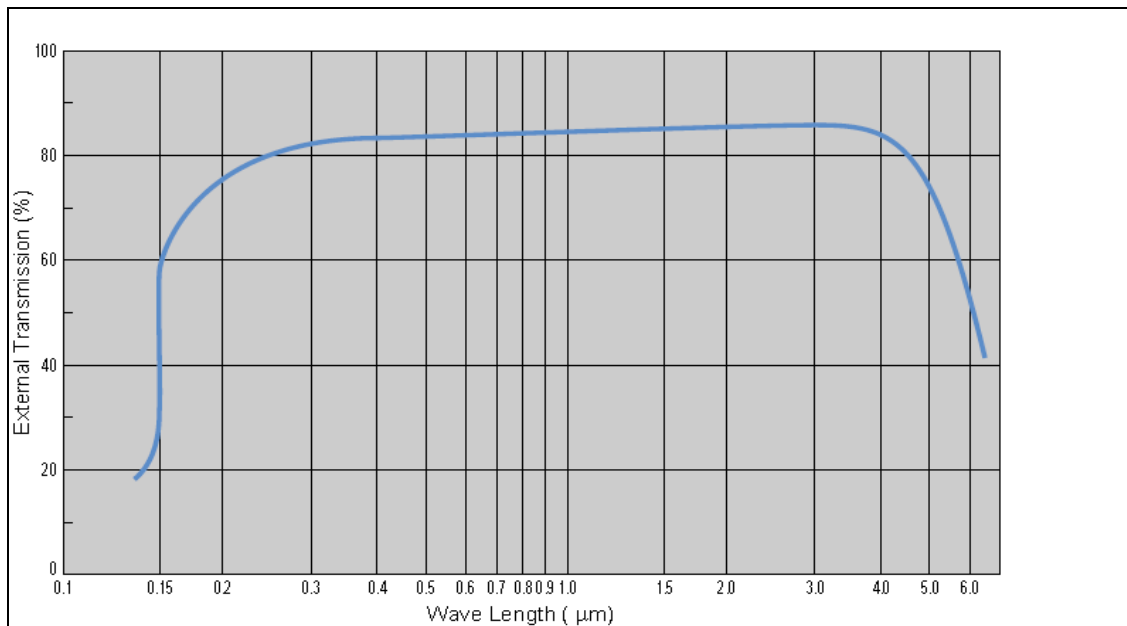


**Figure 2-1. Transmittance range of 0.25 mm thick Sapphire window.** Range of transmission for a 0.25 mm thick sapphire crystal, clearly indicating an increased level of transmittance for the visible spectrum.

## 2.2.2 Window Size

The next element is the thickness and diameter of the pressure windows. As discussed earlier, the volume of the cell is 1 ml, hence the windows must have a diameter of 1.23 cm

or greater. Considering 25% of the windows will be used for sealing and clamping, the windows must have a diameter greater than the required specification. We chose windows with 1.725 cm diameter to give more space for clamping and sealing. The optical elements must be thick enough to withstand 200 °C and 3500 Psi, hence we used Yoder's (Yoder *et al.*, 2006; Harris *et al.*, 1999) formula to calculate the least thickness required, for clamped sapphire windows, with 1.725 cm diameter and a 90% clear aperture.

$$t_w = 0.5A_w[K_w f_s \Delta P_w / S_f] \quad (2.3)$$

Where  $t_w$  is the thickness of the window-which is to be evaluated,  $A_w$  is the unsupported aperture diameter- which in this case is 90% of the clamped diameter,  $K_w$  is a support condition constant and is equal to 1.25 if the window is unclamped and 0.75 otherwise,  $f_s$  is the factor of safety and is considered to have a value- 4,  $\Delta P_w$  is the differential pressure- which in this case is considered to be 3485.3 Psi (3500 Psi – 1 atm),  $S_f$  is the material fracture strength and is 300 MPa for Sapphire (Dunn *et al.*, 1966).

$$t_w = 0.5 \times 0.9 \times 1.725 [0.75 \times 4 \times 3485.3 / 43511.31] = 0.1865 \text{ cm}$$

A window of diameter 1.725 cm and thickness 0.2 cm was chosen as the optical element for the cell.

## 2.3 Sensor

Equilibrium phase diagrams of polymer-solvent systems, represents the polymer composition as a function of temperature. A sensor to detect the temperature along with a system to detect phase transfer are basic requirements. A thermocouple or thermistor that is small enough to be in contact with the liquid and not hinder the light path, or disrupt the sealing, and is able to sense high temperatures is critical to this design. Thermistors usually have a longer response time (10-20 s); and a larger probe which is more difficult to handle.

Hence a thermocouple was preferred. A thermocouple is a junction between two metals (usually alloys) , that produce a voltage proportional to the temperature difference which is read by a multimeter.

### 2.3.1 Type of Thermocouple

There are many different types of thermocouples, each differentiated by chemical properties, melting point, stability, sensitivity and output range. Since our operation range was quite small (25 °C to 200 °C), more importance was given to the sensitivity of the thermocouple. The table below lists the different types of thermocouples and their sensitivity ranges (Beer *et al.*; 1981).

Number	Type(ISA)	Temperature range (°C)	Sensitivity( $\mu\text{V}/^\circ\text{C}$ )	Material
1	E	-270 ~ 1000	60.9	Ni-Cr & Cu-Ni
2	J	-210 ~ 1200	51.7	Fe & Cu-Ni
3	K	-270 ~ 1350	40.6	Ni-Cr & Ni-Al
4	T	-270 ~ 400	40.6	Cu & Cu-Ni
5	R	-50 ~ 1750	6	Pt & Pt-Rh
6	S	-50 ~ 1750	6	Pt & Pt-Rh
7	B	-50 ~ 1750	6	Pt-Rh & Pt-Rh

**Table 2-3. List of different types of thermocouples.** From the above table it is clear that type E and J are more sensitive. Type J thermocouple was chosen based on cost efficiency.

## 2.4 Heat Source

Heating element is the most critical part of the design. Heaters were chosen based on type, size, temperature range, power density, wattage tolerance, lead insulation, and resistance.

### **2.4.1 Type and Size**

Cartridge heaters can be inserted into drilled holes, to heat metal blocks. Also, they provide high wattage in limited spaces, last longer, have a higher dielectric strength and shock and vibration resistance, hence were ideal for our study. The width of the channel is 1 cm (which is the path length), thus there is a size restriction on the type of heating element. Cartridge heaters are usually a few centimeters in length and a few millimeters in diameter, hence it was an obvious choice. We chose to use heaters that were 1.5" in length and 0.12" in diameter, leaving enough room for the holes to be drilled on the metal.

### **2.4.2 Wattage and Watt Density**

Cartridge heaters have a coiled resistance wire wound through a core, and the assembly is covered by a sheath, and they are all rated by wattage and Watt density for either 120 V or 240 V operation. We chose the highest rated heaters for the required size, also because wattage can always be derated if need be, and a good power density was required for homogenous heat transfer. Heaters had a power density of 50 W/in<sup>2</sup> and a rating of 25 W for 120 V.

### **2.4.3 Other Specifications**

The tightly compacted refractory insulation around the coils, provide an excellent heat transfer to the stainless steel wall, which is responsible for resistance against corrosion. The coil is made of ceramic and is wound by nichrome wire, and has a maximum temperature of 677 °C. The leads are made of insulated teflon. A tight fit is required for good heat transfer, hence the holes were drilled in accordance to the diameter of the heaters. The heaters were purchased from Omega Engineering, and the product code is CSS-01125/120.

## 2.5 Insulation

Insulating the metal surface to make the instrument easy to handle, and prevent heat loss to the surrounding was imminent. After considering different insulating materials, we decided to use a hollow block of stainless steel for outer support and connect the aluminium cell to the stainless steel using nuts and bolts. This will make use of air's insulatory properties, and also makes it easier to handle. Since the contact between the two metal surfaces is via small nuts, the heat transfer will be minimal. The following figure gives the cross-sectional view of the use of the hollow stainless steel block.

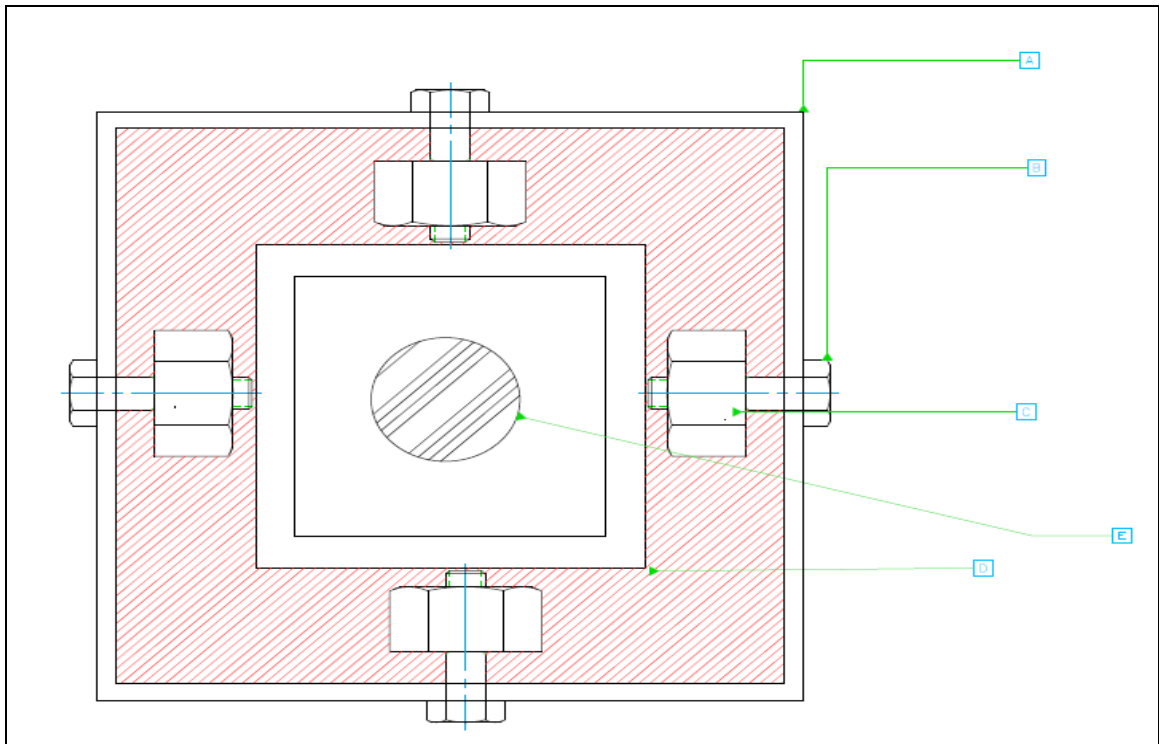


**Figure 2-2. Cross sectional front view of the arrangement.** The above is a cross sectional diagram of the arrangement, A is the stainless steel block, B is the hex screw, C is the nut, D is the aluminium block and E is the solution chamber.

## 2.6 Sealing

Keeping the chamber air tight is a critical part of the design, and hence it is important to seal the windows to the metal, well enough to withstand the high temperature and pressure. The windows are clamped to the metal, with the help of o-rings. We chose o-rings that are made out of teflon- a polymer that can withstand high temperatures ( $-23\text{ }^{\circ}\text{C}$  to  $325\text{ }^{\circ}\text{C}$ ). O-rings help in accommodating any changes for expansion of the metal, or the sapphire windows, giving more flexibility in sealing. The figure below is the cross sectional front view of the sealing and the use of o-rings.

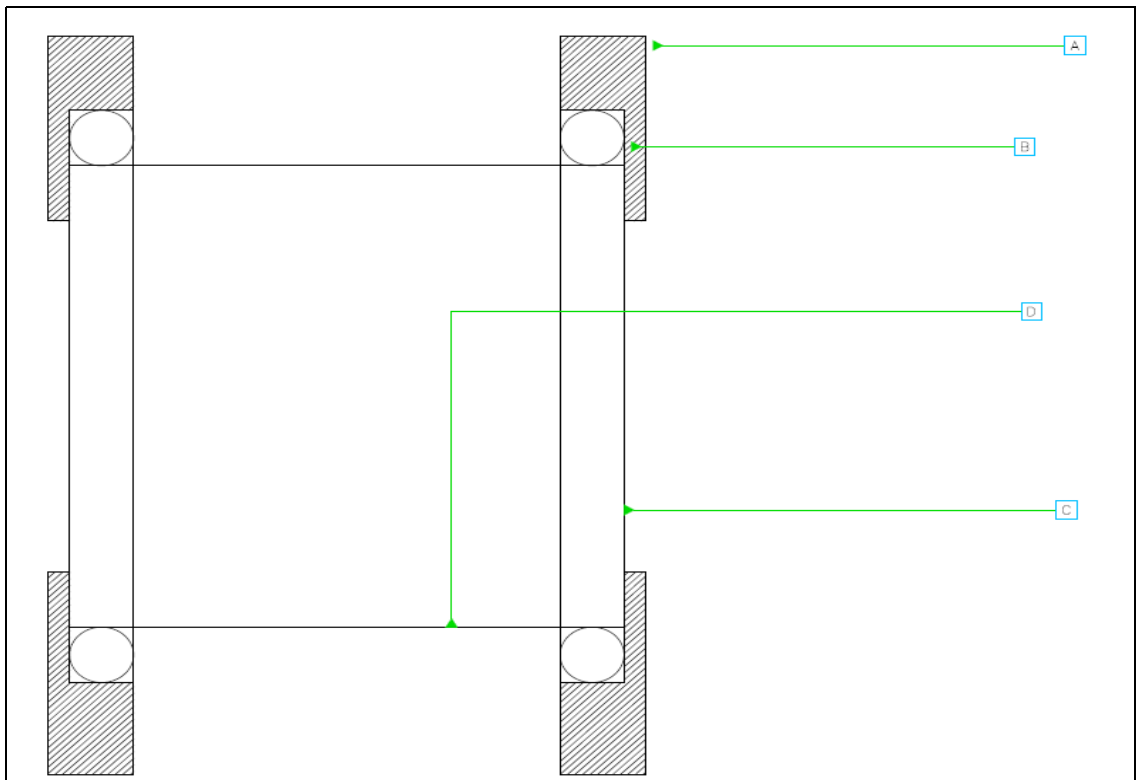


**Figure 2-3. Cross sectional front view of the clamped windows.** The cross sectional diagram of the arrangement where, A is the metal, B is the teflon gasket, C is the window, D is the solution chamber.



## 2.7 Construction

The device is constructed using an aluminium block (5 cm x 5 cm x 1 cm) as the core, a hole is drilled onto the center of the slab. Flanges are made on both sides of the metal piece to accommodate the windows and the o-ring. To prevent leakage and to add pressure to the window-metal interface, another circular metal piece is connected to the aluminium block by screws. Two holes are drilled onto the metal block to accommodate heaters. The heaters are connected to a voltage stabilizer and the heaters are maintained at constant potential difference, to ensure a steady flow of current. The thermocouple is inserted through the inlet port. A hole is drilled onto the center of the chamber, and this acts as the inlet to the chamber, and to keep the setup air-tight, a swage lock fitting was used at the inlet port. The swage lock fitting is a leak tight fitting, that will withstand high pressure, vibration, vacuum and temperature changes. It consists of a cylindrical tube, fitted with a nut and a fitting block that sits on the ferrule. The fitting block and the cylindrical tube is used as an inlet.. We also wrap the ferrule with tape to ensure tighter sealing. The figure below describes the components of the fitting.

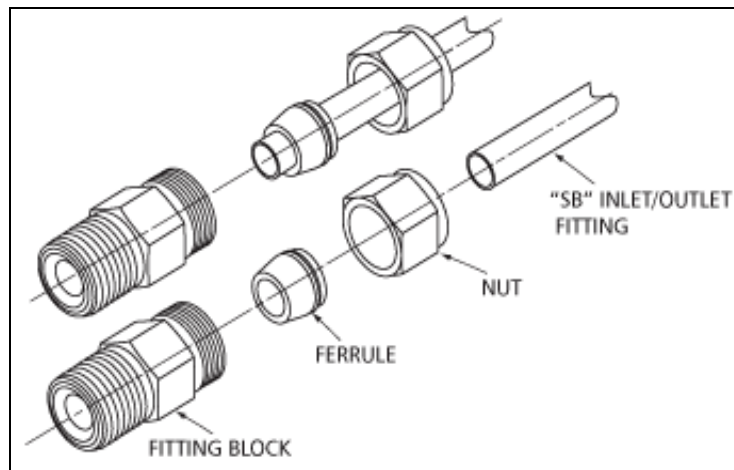


**Figure 2-4 Swage lock fitting:** Three dimensional diagram of the swage lock fitting, consisting of a fitting block piece, that rests on a ferrule, which fits to a cylindrical tube, used to inject the sample.

Swage lock fitting also allows for the insertion of thermocouple into the chamber, the thermocouple is sealed onto the fitting using epoxy. The epoxy was chosen to withstand high temperature conditions, resist moisture absorption and electricity, possess physical strength and chemical resistance, and was purchased from MG Chemicals, product code: 832HT.

### **2.7.1 Steps for Construction**

The following are the steps involved in the construction of the device, describe the arrangement of the above mentioned materials.

a) Aluminium block was ordered from the online metal store, the slab was cut to required dimensions (5 cm x 5 cm x 1 cm) and a hole of 1.25 cm diameter is drilled onto the center of the slab. This space acts as the solution chamber. Flanges of a few centimeters are milled on both sides of the block, to accommodate o-rings and the windows. Two channels, 0.15" in diameter and 1.5" in length are drilled on either side of the center chamber to accommodate the heaters.

b) A circular plate of diameter 4 cm was cut from the slab, and a hole of 1cm was drilled onto the center of the plate. Six hex screws (4-40) are used to screw the circular plate onto the metal block.

c) The swage lock fitting is fitted on the top of the metal block- above the drilled center hole, after drilling a 1/8" hole for the cylindrical tube, the ferrule was locked onto the epoxy coated tube.

d) The heaters were connected to the voltage stabilizers, using the lead leads and the thermocouple was connected to a digital temperature monitor. The following figures explain the final design in detail.

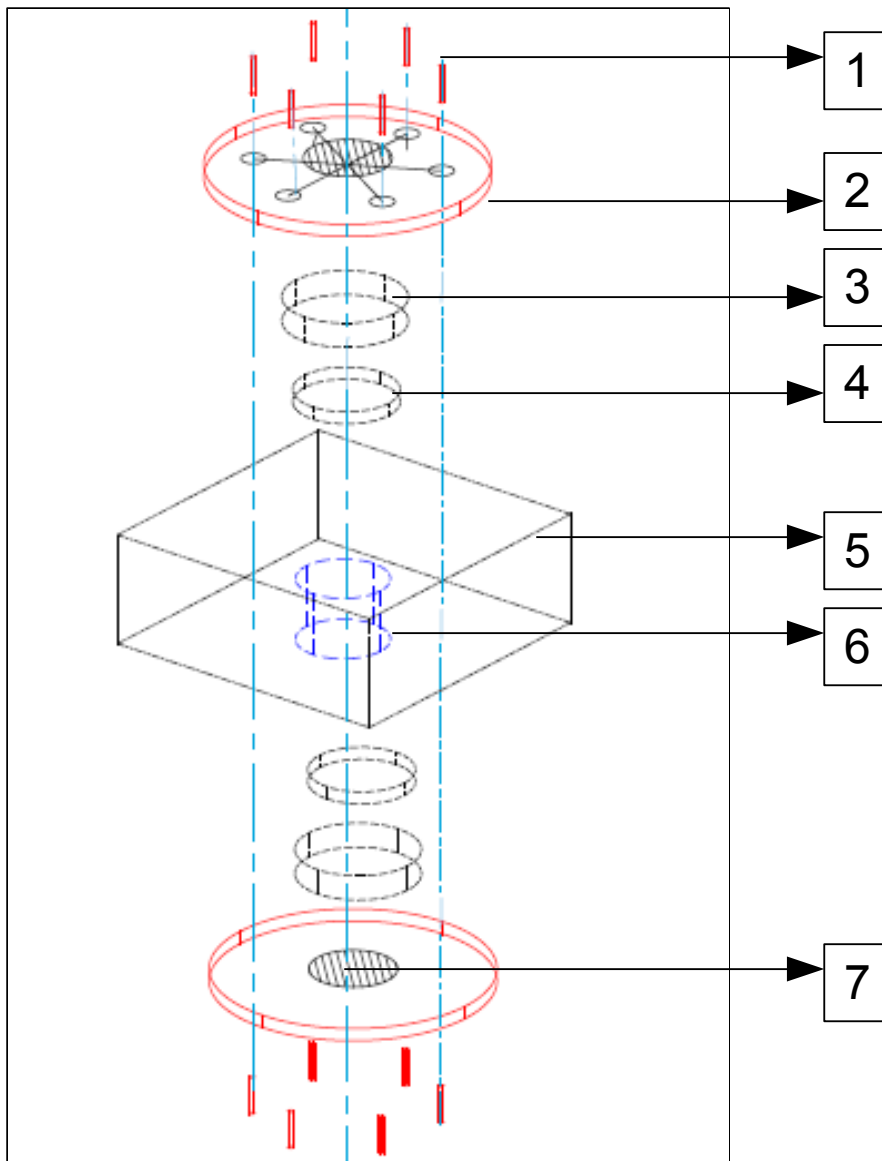


**Figure 2-5. Complete view of the cell alignment.** A detailed step by step drawing of how the device was put together. 1 represents the pins/screws, 2 is the circular plate, 3 is the sapphire windows, 4 is the o-ring, 5 is the metal block, 6 is the solution chamber 7 is the hole in the circular plate.

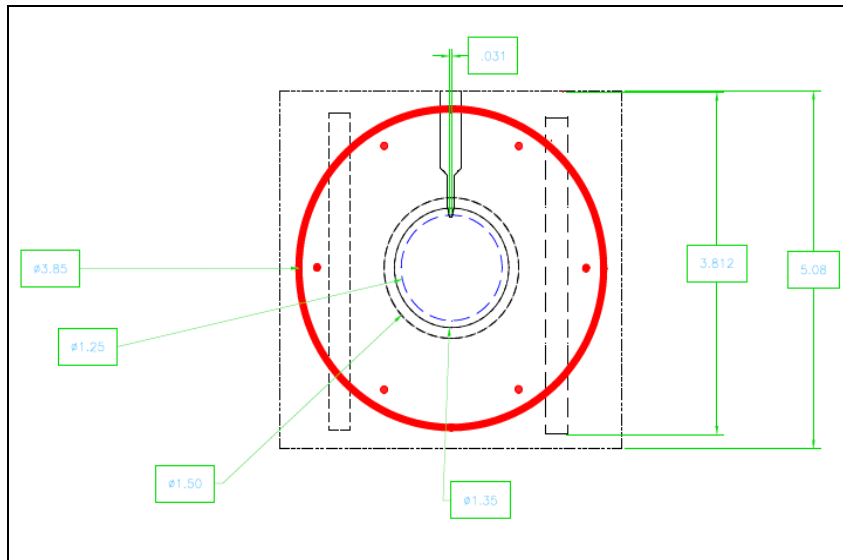


**Figure 2-6. Cross sectional front view.** Front view of the device and it is drawn to scale, with exact measurements. The slot for the heaters are in dashed lines.

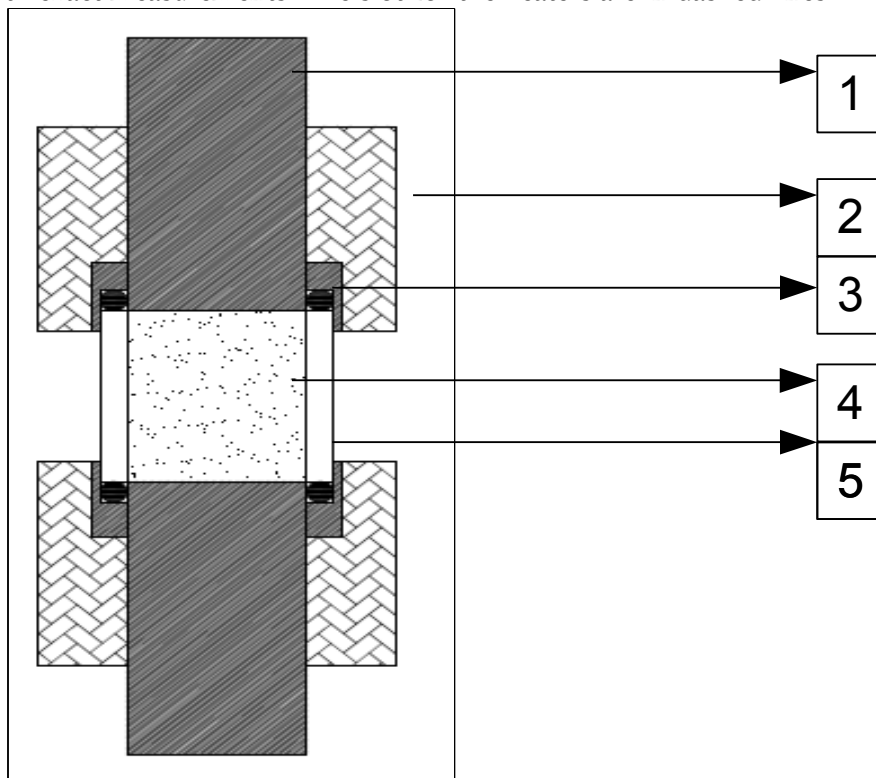


**Figure 2-7. Cross sectional left view.** Left view of the device drawn to scale, with exact measurements. The slot for the heaters are in dashed lines.

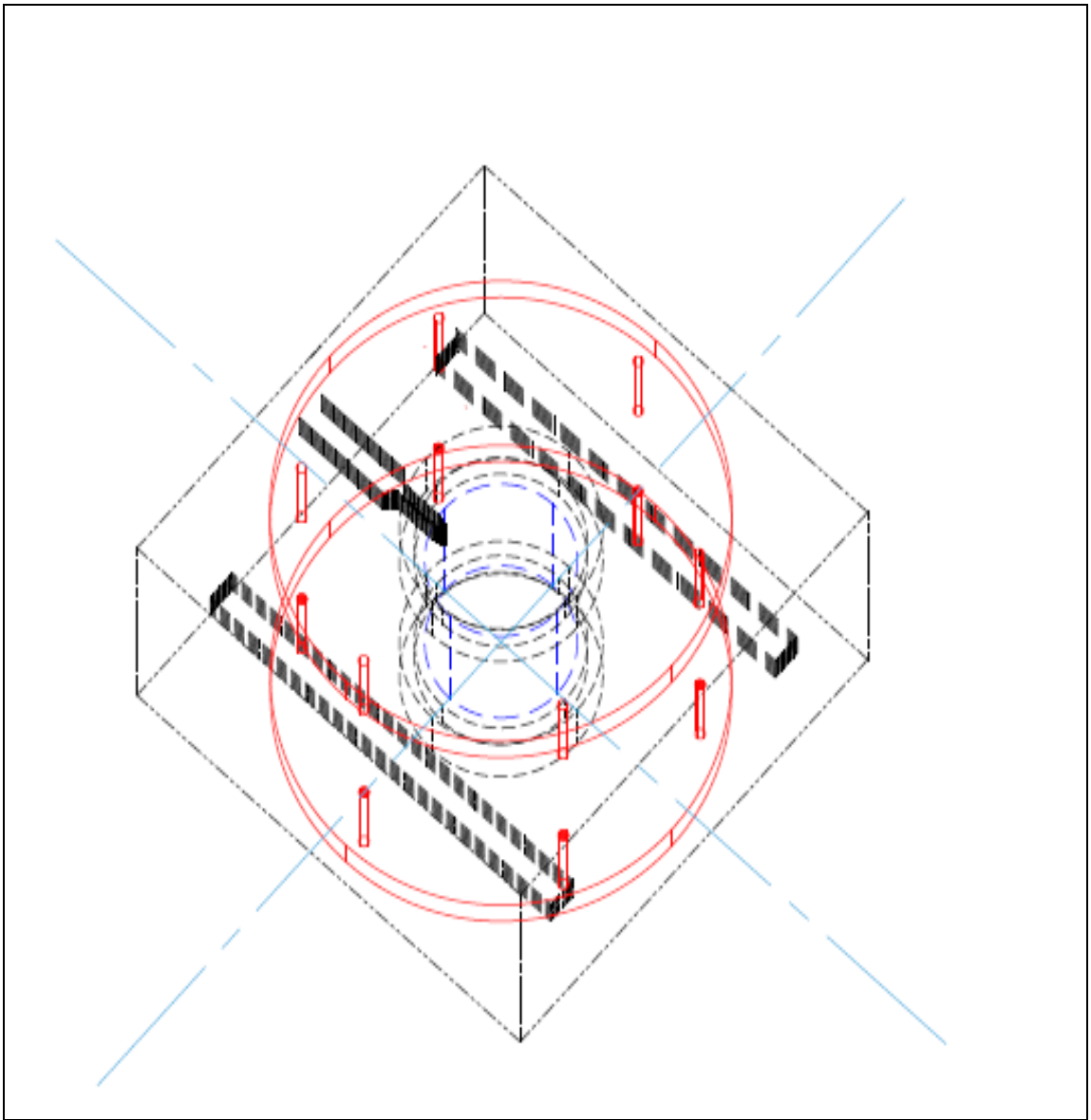


**Figure 2-8. Isometric view.** Isometric view of the design from the south-west direction.

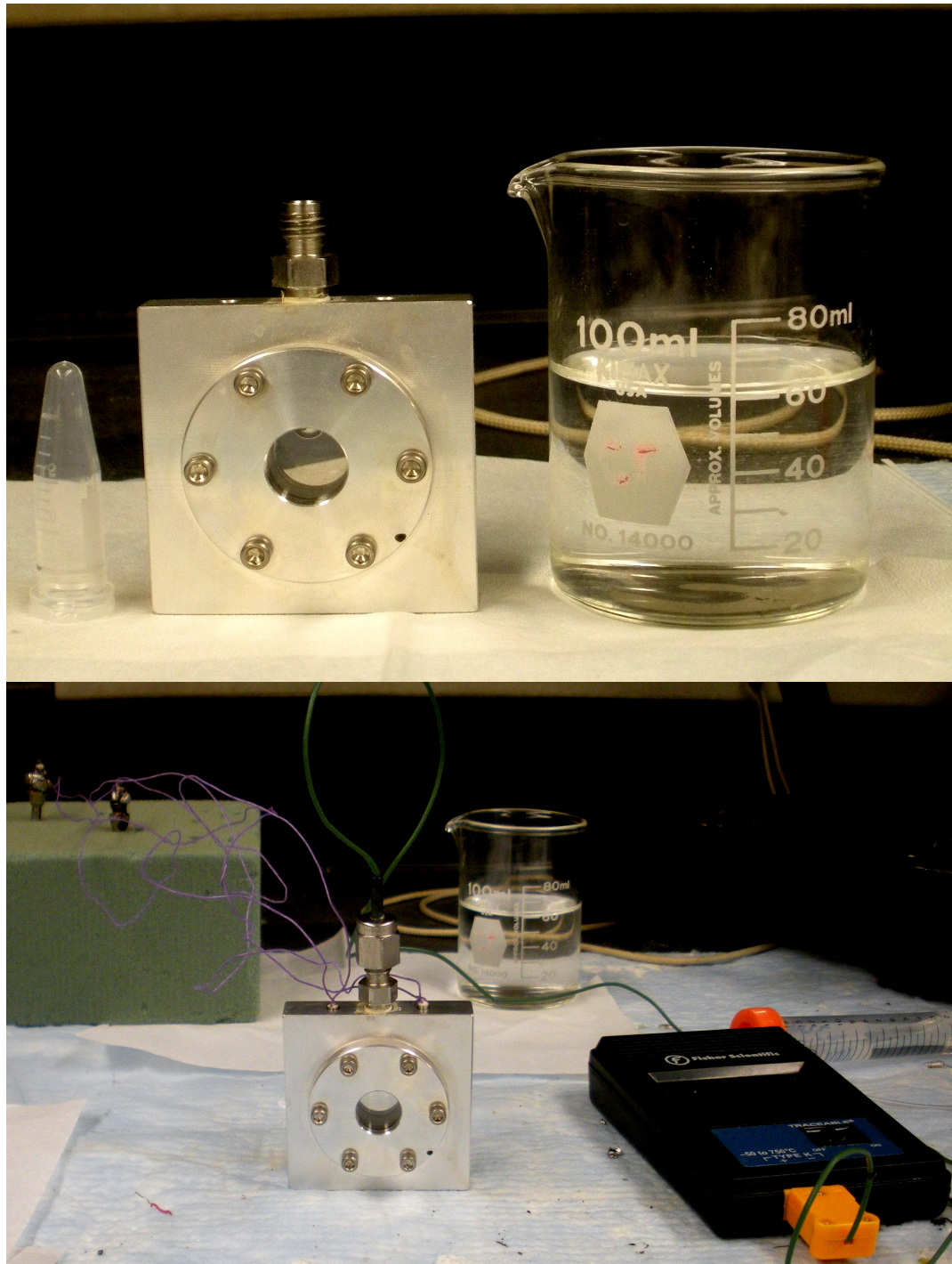


**Figure 2-9. Image of the device.** (Above) Image of the device with a 1.5ml eppendorf tube and a 100ml beaker for size differentiation. (Below) Cell connected to heaters (leads grounded) and thermocouple.

## Chapter 3

### Detection and Analysis

We integrate the cell with a absorbance/turbidity based detection system as mentioned previously. The light source used is a mercury lamp and next to the lamp is a filter, that filters 50% of the light, and a diffuser followed by a pin hole adjustment. The cell is fixed on to an optical desk, in front of the pin hole adjustment, a camera is fixed next to the cell. The camera is connected to a computer for data acquisition. Videos are recorded using VirtualDub, a software, and analysed in MATLAB. The following block diagram is a good representation of the arrangement.

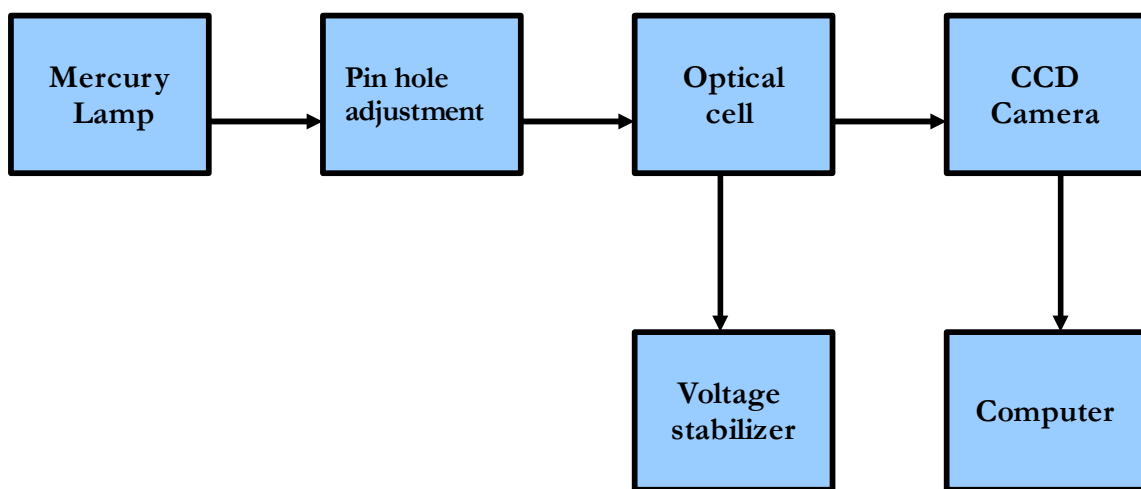


**Figure 3-1. Block diagram of the arrangement.** Arrangement of the detection system and how the experiment was carried out. Mercury lamp was used as the light source out of convenience and availability. The experiment was carried out by adding the test solution to the cell and supplying a constant voltage. After the movies are recorded, they are edited on video editor, and analyzed in MATLAB.

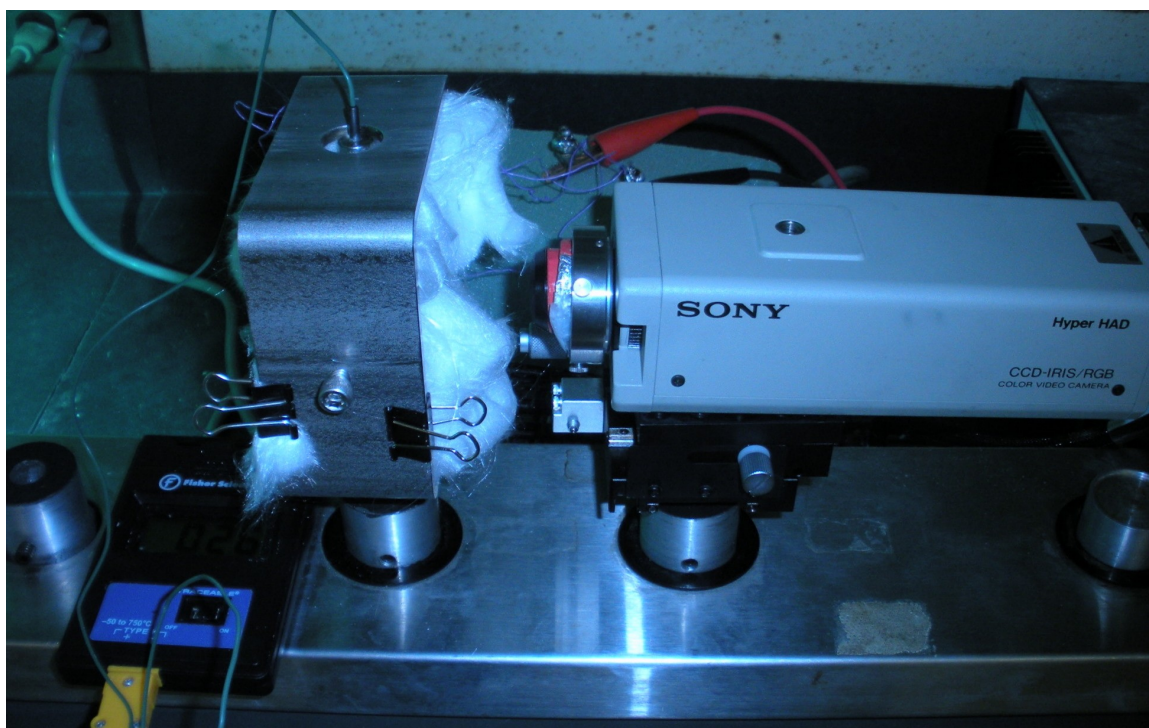
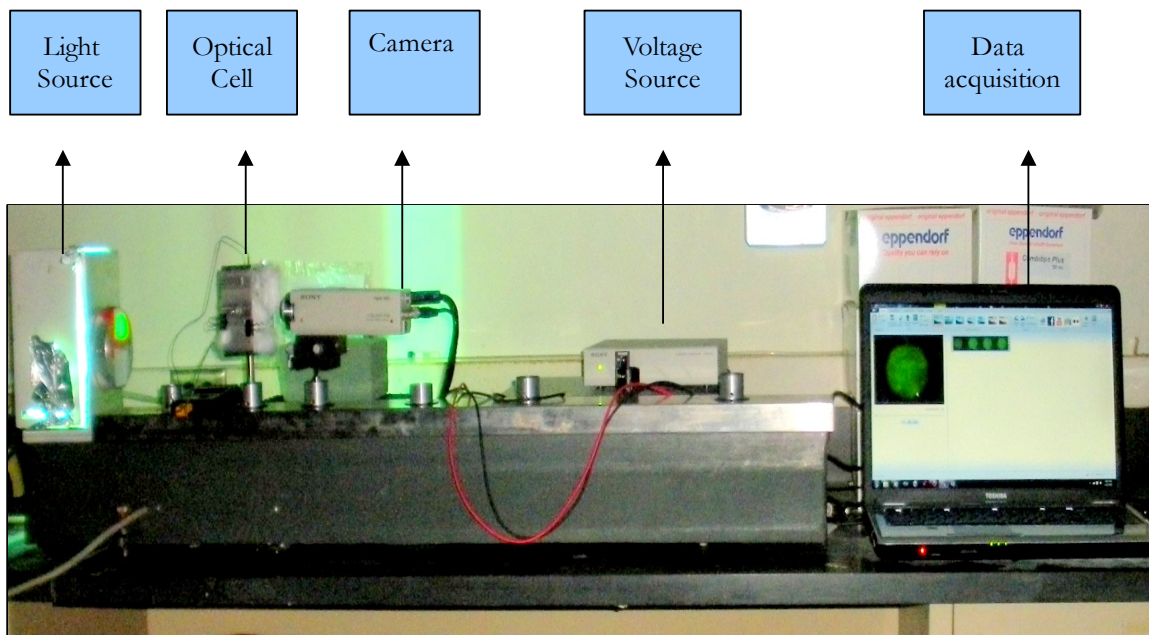


**Figure 3.2. Image of the setup.** (Above) Arrangement of the detection system. (Below) Zoomed image of the cell, covered by glass wool, connected to the thermocouple



Green light is used to detect turbidity, and cloudiness is detected as a decrease in intensity of green light. We perform initial intensity analysis on a completely clarified liquid (water) and a completely cloudy liquid (concentrated milk), to get an idea of the change in intensity due to turbidity and also the sensitivity of the system. Apart from transmittance, we also capture real time videos to understand the individual process, once a change in absorbance or transmitted light is observed. Since studying phase transitions and the process of aggregation is part of the objective, a direct observation of the process, in case of a change in transmitted light is essential. This is achieved by changing the source to white light and observing the changes on the CCD cameras. We use reflected light for direct capture and add in a 4X objective for focussing, also we place the camera on a micrometer stage to help in the same. By using this method, we can cross check the reasons for change in absorbance, and observe the process of changes responsible for an increase in turbidity.

The cell is cleaned with double distilled water, sonicated and rinsed with methanol. It is later vacuum dried, or dried in the oven at 150 °C for a few minutes. Aggregates of the proteins can adhere to the windows, and the cell is cleaned by sonicating the cell with RBS inside, or dilute acid. The cell can also be dismantled and re assembled if required, to replace any part of the cell.

A syringe is used to add and remove samples. The voltage stabilizer maintains a constant wattage of 20 W. The wattage can be lowered or the current kept constant, to observe changes at a particular temperature.

### 3.1 Image and Intensity Analysis

Green light from the mercury lamp was used as the light source. When the liquid is clear, we can observe a circular green spot on the screen, and as the temperature is increased, and when the mixture begins to cloud, the incident light leaving the cell produces a dimmer image as seen below. The following are pictures of the cloudy mixture and a clarified liquid.

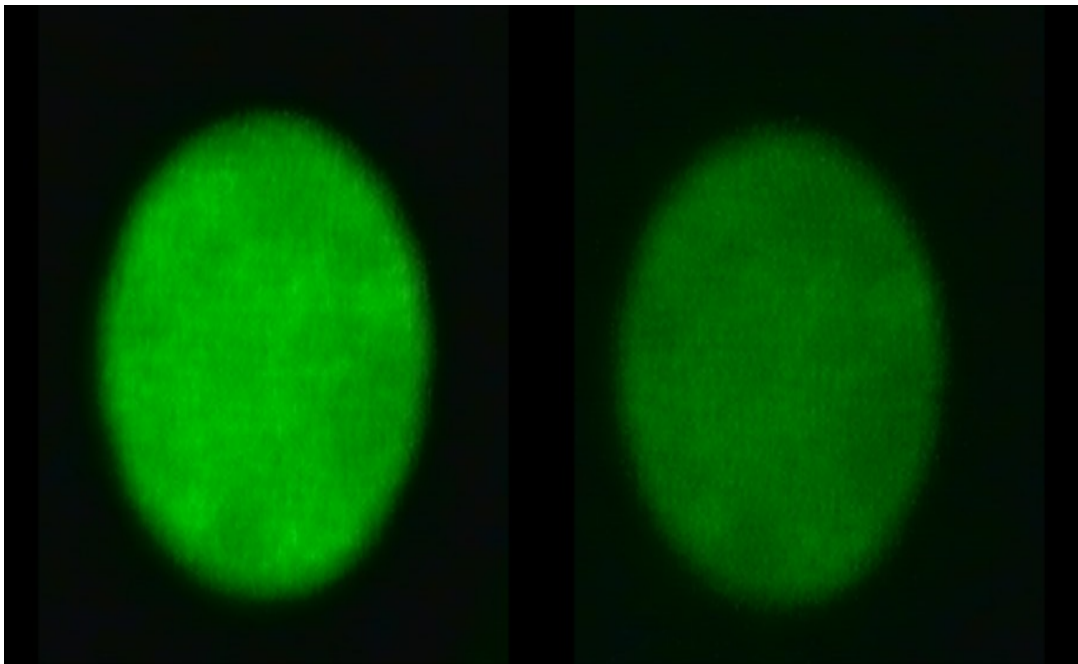


**Figure 3-3. Image of the video output.** Two recorded images, the one on the left is the light, after passing through a clarified liquid. The one on the right is that of light, after passing through a cloudy sample. Analyzing the intensity profiles of the above images will give us more information on the turbidity. Also, the blank image is a completely black image. All the results are normalized with respect to the blank image.

### 3.1.1 Analysis in MATLAB

The following is the algorithm for analyzing the movie files. The movies recorded are in .avi format, noise value is calculated from a blank movie file. The videos were recorded using the software Virtual Dub, the videos were in yuy2 format, which is the format associated with webcam video files. MATLAB can read only the RGB formatted files, hence it is necessary to change the format of the video file, before loading it in MATLAB for further analysis. The recorded video were of the size 640 x 480 pixels ,and 30 frames were recorded per second to make the video. The following is the algorithm used for intensity analysis.

- a) The total number of frames are determined, after reading the movie file in “.avi” - RGB (red green blue) format.
- b) The movie is converted to the number of frames and the information of all the frames are stored in a separate file.
- c) Intensity of black is zero and white is one. We extract information of pixels that have an intensity value greater than zero, and add it on to a new file with the noise value previously determined.
- d) Analyze the new file, and sum the intensity values of each pixel of the 640 x 480 image.
- e) Plot the intensity values of each frame with time.
- f) Further analysis of different frames can be performed.
- g) For coloured video files, the files were converted to black and white before analysis.

## 3.2 Characterizing the Detection Setup

It is important to characterize our detection system, hence a few basic experiments were performed using milk as the sample. Milk contains an innumerable number of dissolved particles, and is also an emulsion of a continuous colloidal phase. Hence the right sample to test the system. Two ml of two percent milk was taken and serially diluted (20 fold), and each of those samples were tested for turbidity using our system, the video files were recorded for half a minute and the total intensity analyzed. Also, the absorbance values of the same samples were obtained using the spectrophotometer. The results obtained from both the experiments correlated with each other, with not much difference. However, our system failed to detect highly concentrated samples due to extreme turbidity, which resulted in a zero intensity plot. Nonetheless, our system was effective in the region of interest and hence can be considered as a good enough scale to detect cloud points. Absorbance values increased with concentration of milk, and the Intensity values(transmitted light) decreased with higher concentrations of milk. The data and relevant graphs are presented below. Observed images are presented in the Appendix.

Ratios of Dilution	Absorbance	Intensity(normalized)
1	2.434	6.9303
0.5	1.941	8.9023
0.25	1.1182	115770
0.125	0.5884	532230
0.0625	0.2902	850540
0.03125	0.1498	1068600
0.015625	0.0727	1217400

**Table 3-1. Absorbance and Intensity values for serial dilution of milk .** List of absorbance values using spectrophotometer and the intensity values obtained by using our detection system for different concentrations of milk.

The ratios of dilution was considered to plot the graphs, and the plots were non-linear. The CCD camera was unable to detect changes in very high brightness or very low brightness, however it was found to be very sensitive in detecting clouding. Most of the experiments that were designed to be performed with this instrument were in the absorbance range of 1-2 and below 0.5, and hence in this range, our detection system was sensitive enough to perform experiments.

From the graphs below, it is clear that there is no clear relationship between absorbance values and Intensity readings. However, there exists a good correlation and even proportionality between the two methods. The relationship between the absorbance and concentration is exponential, and the relationship between the total intensity values averaged over all the frames of a 30 second movie, and concentration is logarithmic.

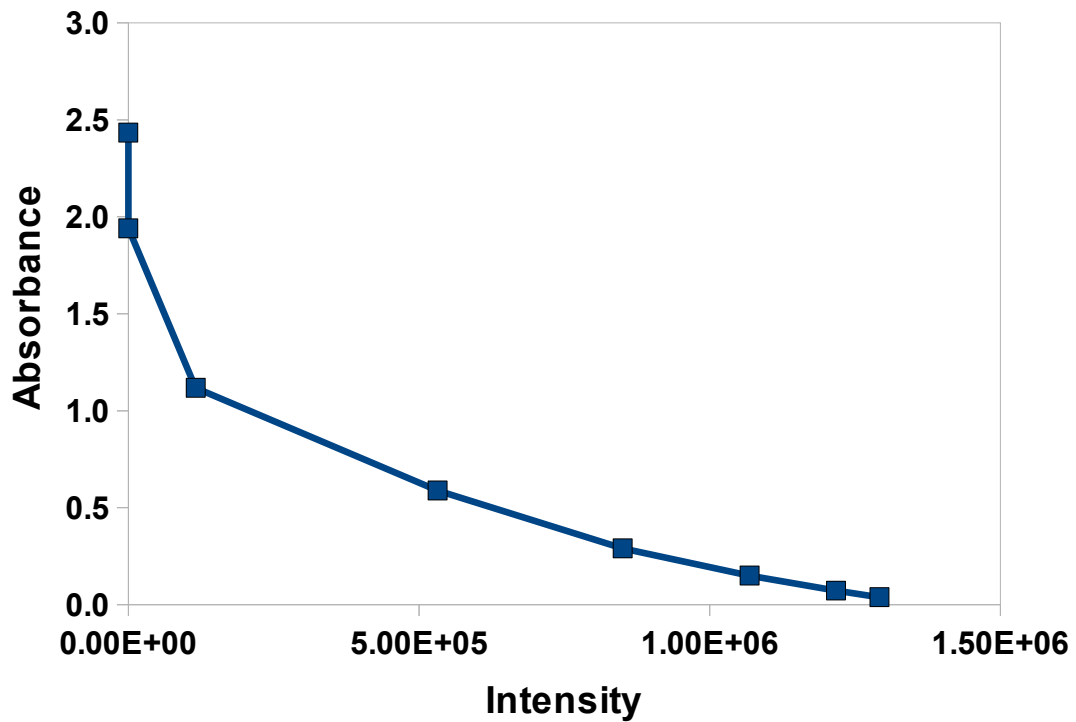


**Figure 3-4. Absorbance vs Intensity.** The Intensity is sensitive, even at low absorbances of 0.1, however, loses sensitivity on increase in absorbance value beyond 1.

We plot absorbance values of each diluted sample with its respective intensity. The above graph is a clear representation of the sensitivity of our detection system. The system is sensitive even at absorbances, as low as 0.1 . And there exists a linear correlation between the absorbance obtained via spectrophotometer and the intensity obtained using video analysis, this lasts till an absorbance value of 1. There is a decrease in sensitivity of the system, beyond this point, however since the objective of this report is to detect cloud points. The sensitivity of the detection setup, over the range of operation and experimentation was very high.

### **3.3 Determination of Cloud Points for PEG(8000)**

We measured cloud points of a PEG-water system. PEG(8000)-water system is a well studied and researched system, hence an obvious choice. The cell was designed to handle a maximum of 200 °C, and the UCST of PEG-8000 is at a much higher temperature, hence LCST was evaluated and the cloud points were plotted. Initially, water was heated inside the cell, and we were able to keep the water in a superheated state, at 175 °C. 10, 20, 30, 40, and 50 percent (weight fraction) PEG-8000 aqueous mixtures were made, and the solutions were heated inside the cell, the videos captured were analysed. The values obtained matched the ones obtained by other theoretical and experimental methods (*Saeki et al., 1973; Bae et al, 1991*). The following is an account of results for a 50% solution, a decrease in intensity is noticeable at a temperature of 146 °C, which drops to zero beyond that temperature. And on cooling the intensity increases again, at the same temperature. Since the process was reversible, it clearly indicated the detection of a cloud point. Firstly, the image analysis of the 50% solution, followed by a complete intensity analysis.

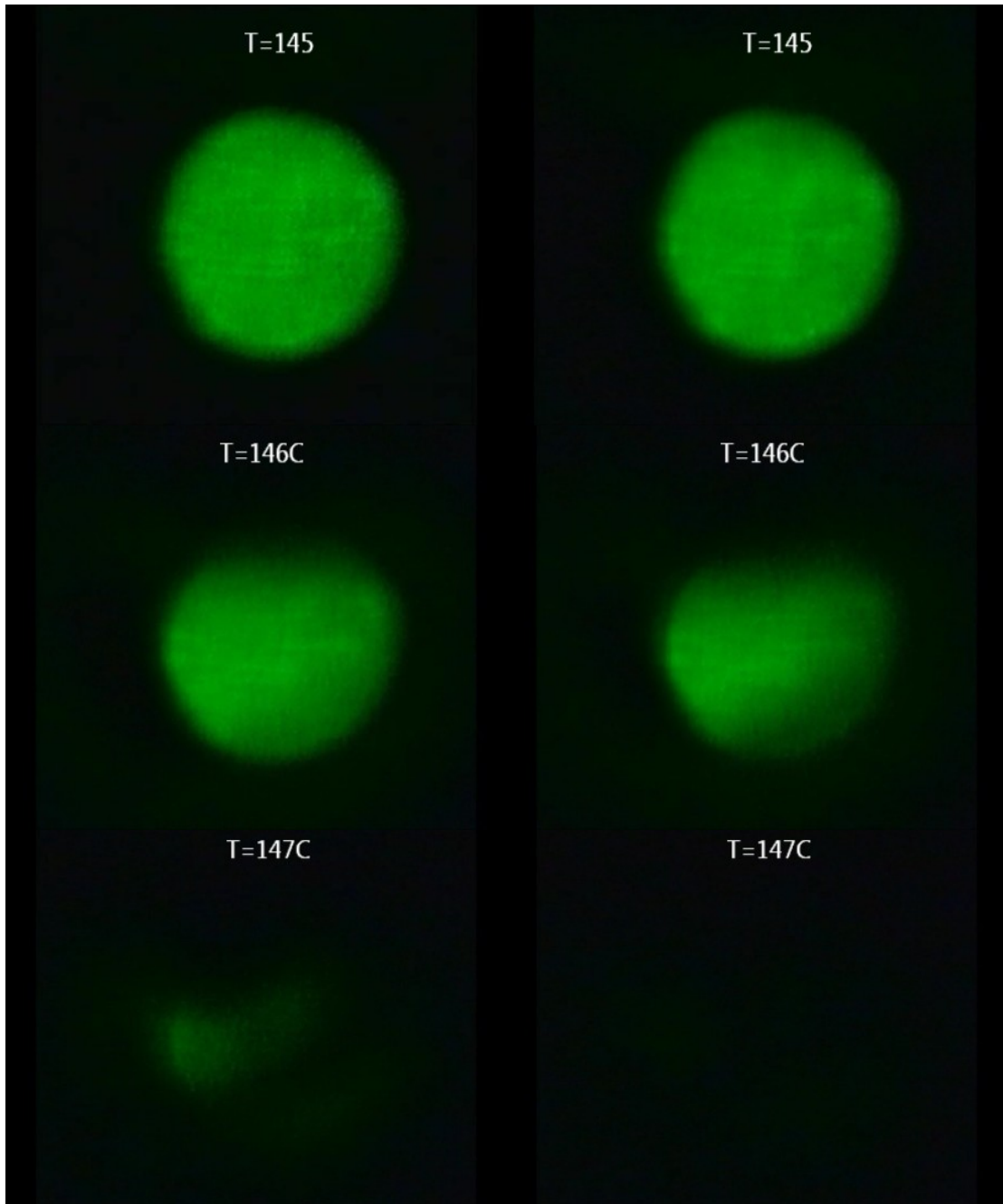


**Figure 3-5. Turbidity of green light.** Image analysis of heating 50% PEG solution. Frames at different temperatures, showing the clouding of the solution. Clouding begins at 146 °C and beyond 147 °C the screen can not detect any transmitted light.

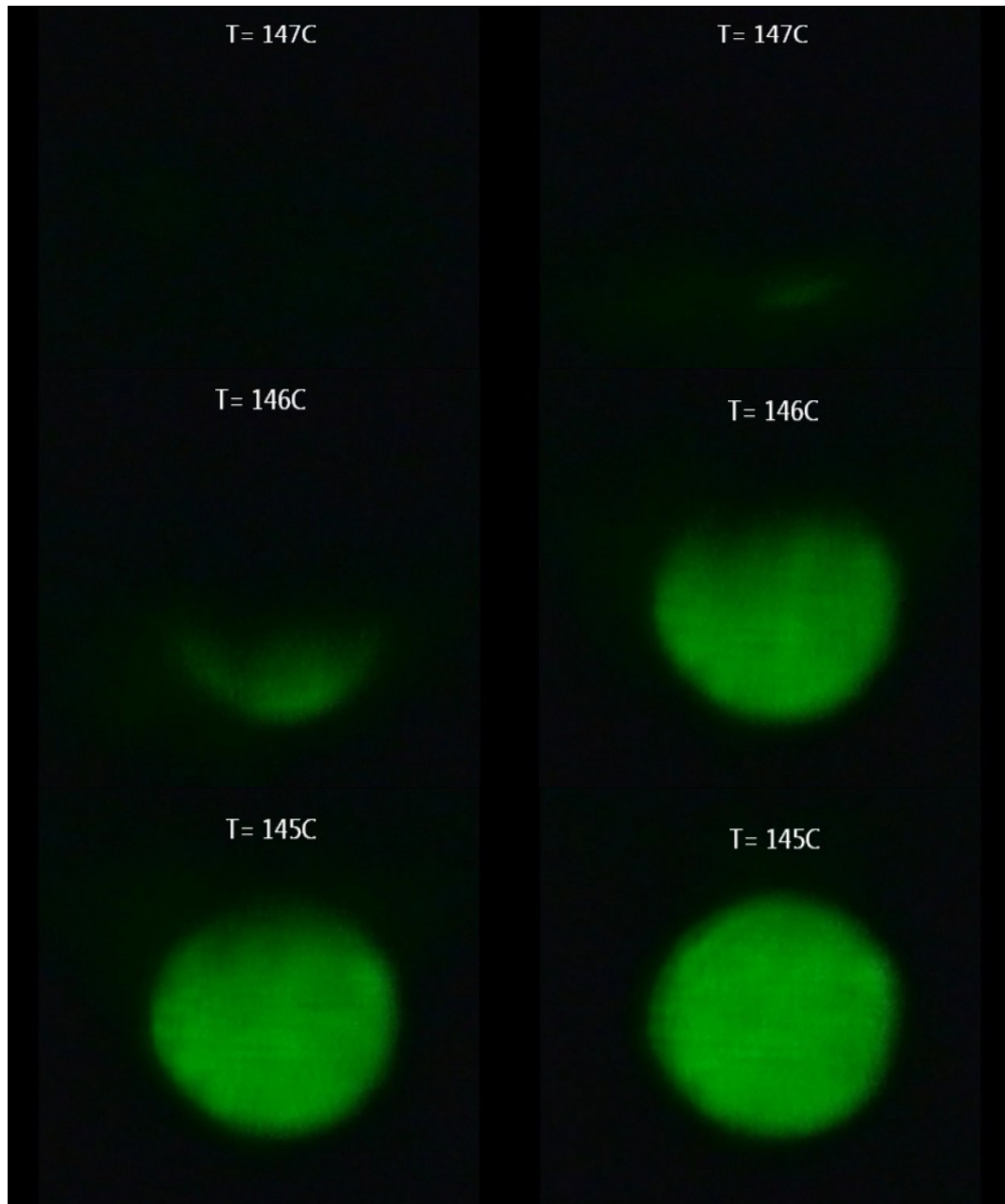


**Figure 3-6. Image analysis of cooling 50% PEG solution.** Frames at different temperatures, showing the clarification of the solution. The solution starts clarifying at 146 °C, and below 145 °C the screen transmits all the green light.



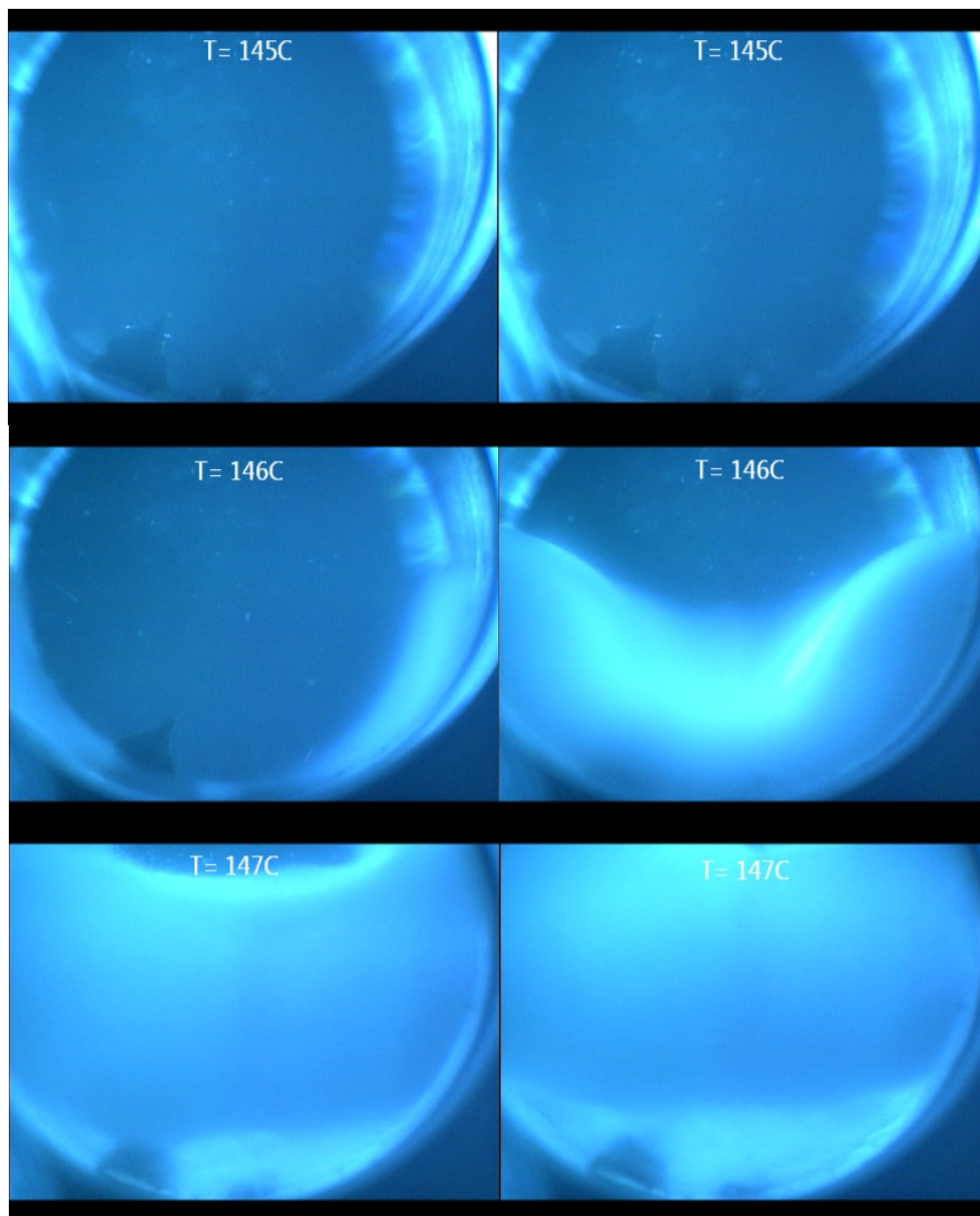


**Figure 3-7. Direct video capture.** Image analysis of heating 50% PEG solution. Frames at different temperatures, each corresponding to a particular absorbance value.

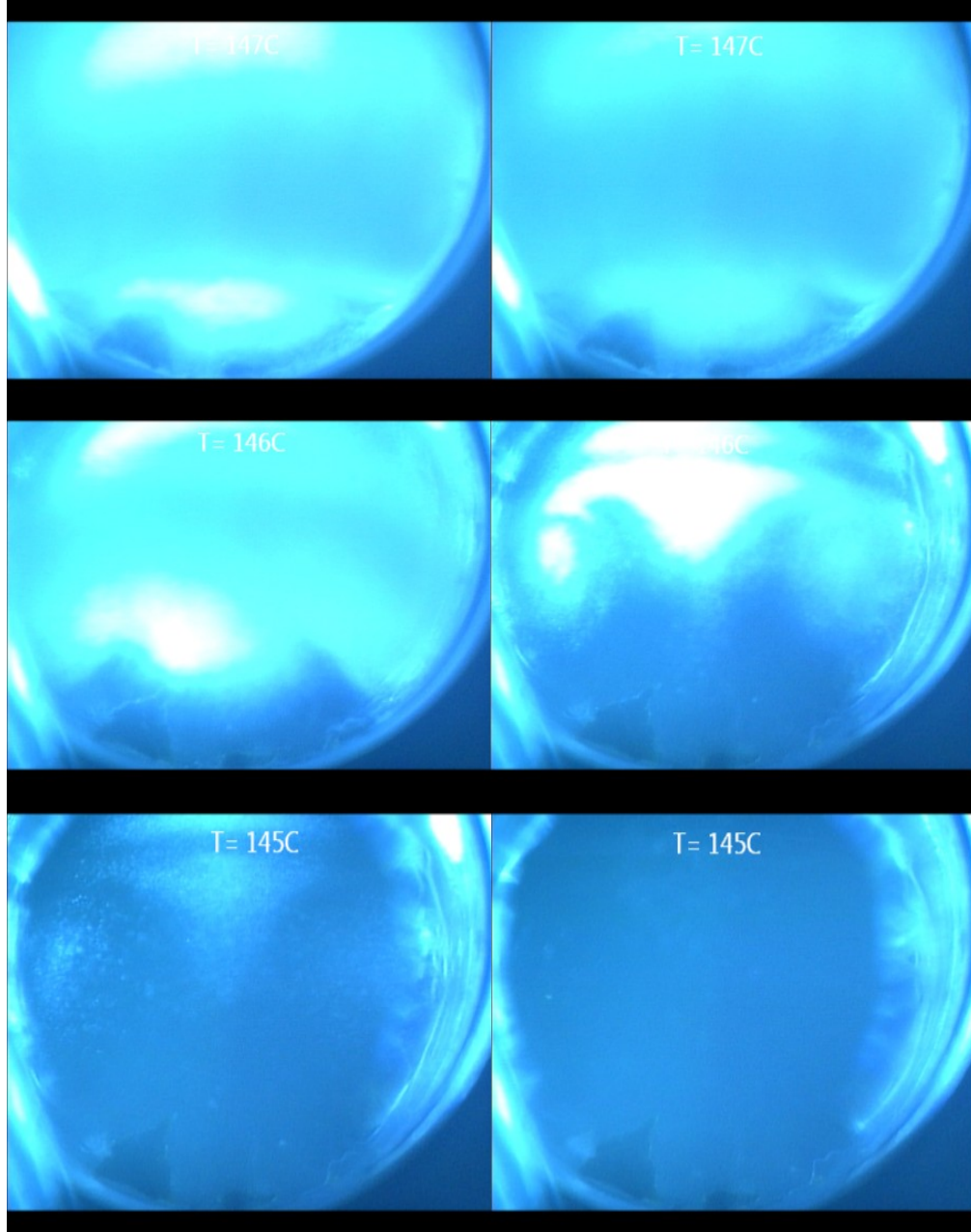


**Figure 3-8. Direct Video Capture.** Image analysis of cooling 50% PEG solution. Frames at different temperatures, each corresponding to a particular absorbance value.

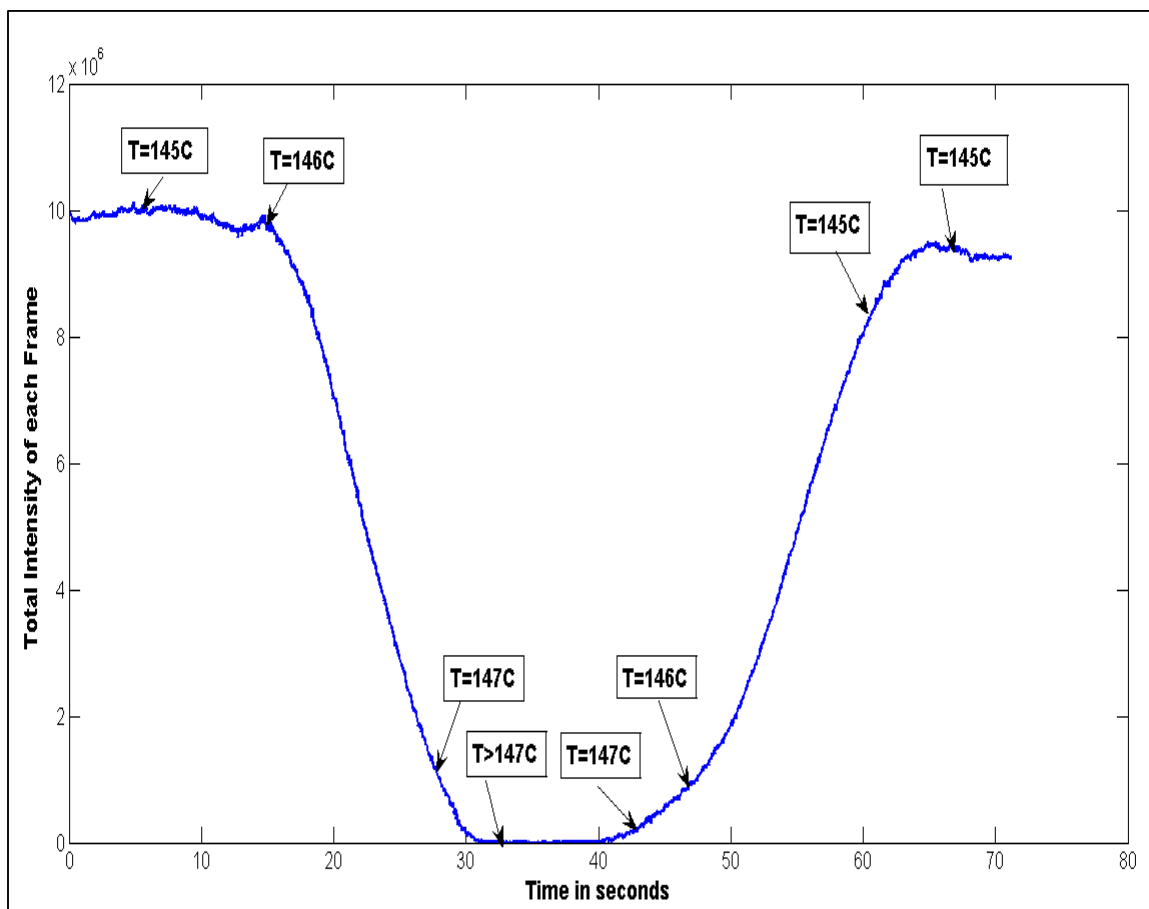


**Figure 3-9. Intensity plot.** Analysis of the heating and cooling of PEG 50% solution from temperature 145 °C to 147 °C and vice-versa. The above graph shows a dip in intensity value at 145 °C, which regains at 146 °C.

Individual plots showing the increase in clouding and eventual clarification are shown below. These experiments were performed for other concentrations and the cloud points were recorded. The plots for each of the concentration is available in the appendix of this record.

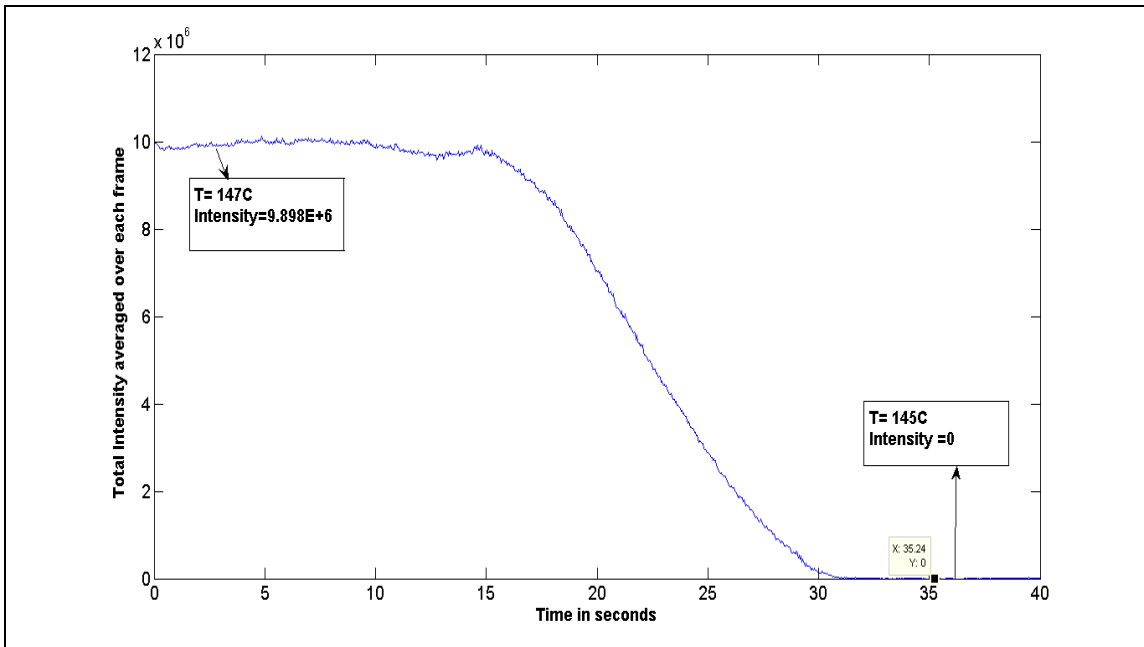


Figure 3-10. Intensity plot of heating PEG solution. Intensity values at respective temperatures.

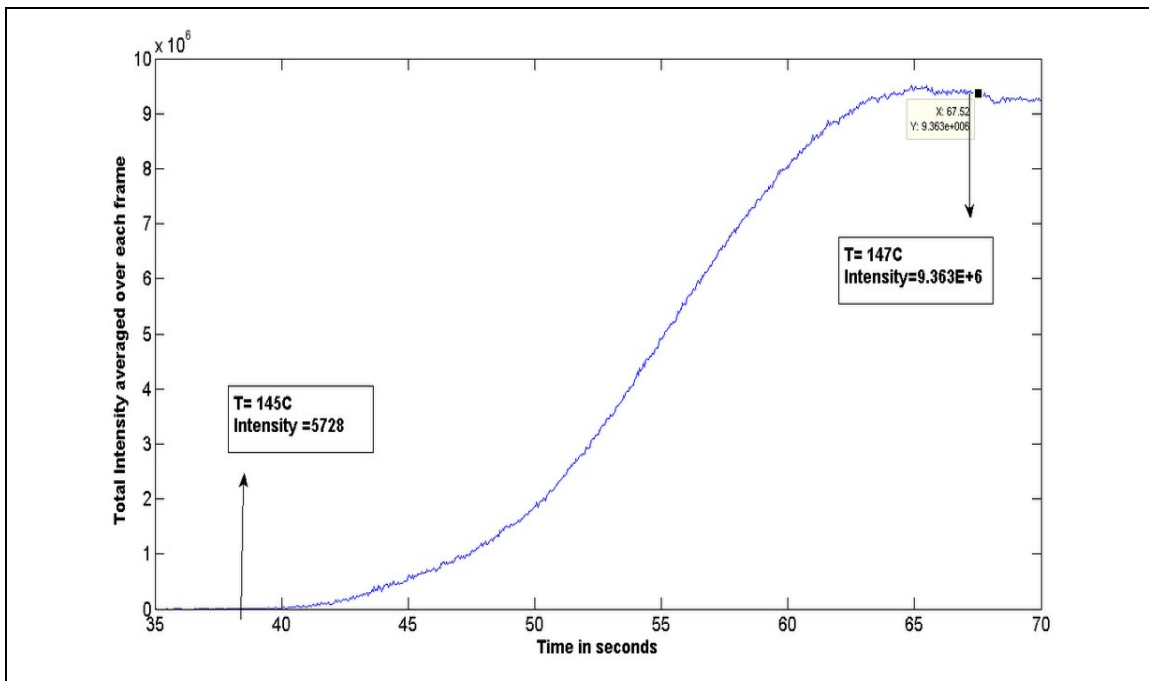
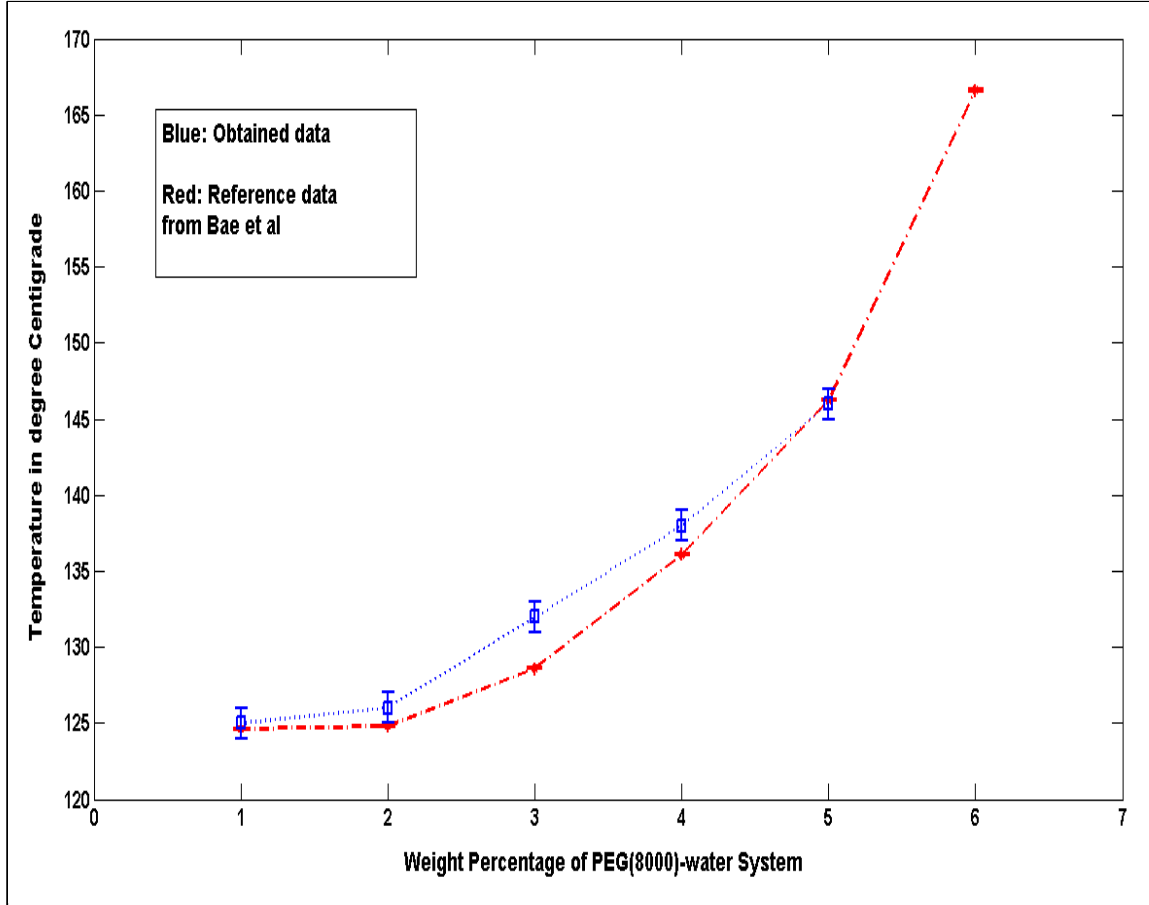
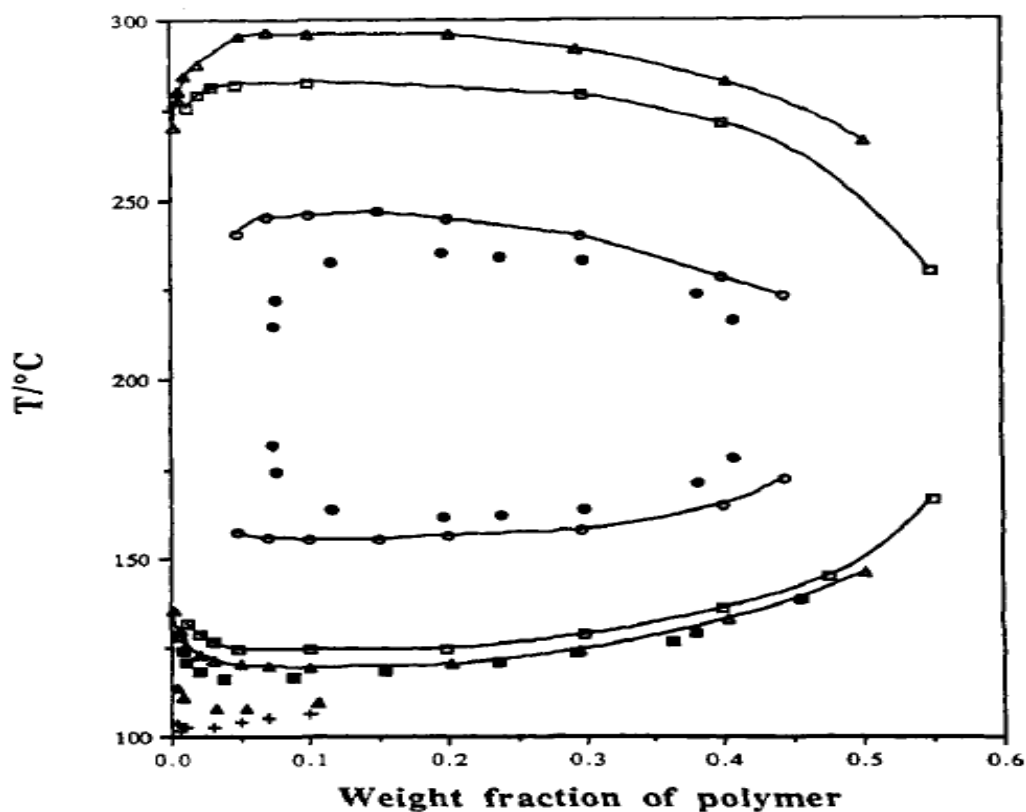


Figure 3-11. Intensity plot of cooling PEG solution. Intensity values at respective temperatures.



**Figure 3-12. Phase diagram of PEG (8000)- water system.** Partial phase diagram of PEG-water system, showing cloud-point temperatures as a function of weight fraction of polyethylene glycol. Blue points constitutes the experimental values, and the red denotes the values obtained from Bae *et al.*

Cloud points were observed for different concentrations of the binary mixture, to plot the phase diagram and determine the LCST of the mixture. This diagram correlates with the one published by Bae *et al.* In 1991. This analysis helps in validating the function of the cell and its use in constructing phase diagrams of other polymer-solvent systems.



**Figure 3-13. Phase diagrams for several PEG-water systems.** A figure, from *Bae et al., 1991*, and displays the UCST and LCST for different PEG-water systems. In the above figure, dark circles are for PEG molecular weight of  $3.29 \times 10^3$ , and the dark squares are for PEG-8000 and the dark triangles are for PEG- $14.4 \times 10^3$ . (Printed with permission)

The above correlation confirms the use and validity of the cell. However, the applicability of the cell for protein aggregation studies remains to be tested. Hence the following experiments were carried out. The images and intensity plots of other concentrations of PEG(8000)-water systems can be found in the Appendix.

## 3.2 Studying Protein Aggregation

Many neurodegenerative diseases are characterized by protein aggregation, the process of phase separation in protein solutions, is due to a range of interactions (*Dobson et al., 2004*). As discussed previously, the phase diagram of a polymer-solvent system provides us with great details on driving forces and mechanisms involved in polymer aggregation. Even partial information on the equilibrium curves can help in better understanding of IDP aggregation (*Crick et al., 2010; Pappu et al. 2007*). Unpublished data reveal that proteins tend to disaggregate in superheated water, and hence appropriate to study the same in a high pressure-high temperature cell.

Domains of polyglutamine are part of various intrinsically disordered proteins and hence are associated with protein aggregation. One millimolar sample of polyglutamine (Q(40)KKKK) was prepared and heated in the optical cell, to understand the possibility of using the cell to study protein aggregation, also to try and gain insights on the critical temperature and phase transitions. Aggregates might not be precipitates but all precipitates are aggregates. Hence the presence of aggregates in solution can only be determined by a quantitative analysis of the size distribution. However, we can identify the presence of precipitates using our analysis, and can possibly integrate the system with a small angle scattering setup upon noticing an interesting change, to understand the complete process.

We also performed similar experiments with CsgA, a curlin subunit of *E. coli* involved in fibril formation. Few aggregating proteins have been suspected to be monomeric at high temperatures, hence heating an aggregated solution, might help us gain critical details on this general perception.

The polyglutamine sample is prepared by dissolving 5.04 mg protein in 1 ml water. The dried sample is dissolved in equal portions of trifluoroacetic acid and 2-propanol, dried by nitrogen

and dissolved in 50 mM, pH 7 phosphate buffer (*Crick et al., 2006*). The sample is heated inside the cell, at a constant wattage of 20 W, and the absorbance changes are recorded. After which, a real time video is subsequently recorded, to better understand the phenomenon behind change in transmitted or absorbed light. The changes that appeared in the system on heating beyond a temperature range, disappear on cooling, and hence can be reproduced in a single trial. At 30 °C, large aggregates of the sample settle at the bottom, and some stick onto the glass. As we heat the sample, during a period of 160 °C to 175 °C, the precipitates settled at the bottom start to disappear. To summarize, initially the solution was completely cloudy, and on increase in temperatures the precipitates settled at the bottom and on further increase in temperature, the settled precipitates started to disappear. The figures below show corresponding direct video images.

A similar experiment with CsgA was performed. Sample was prepared using 20mM, pH 7.2 phosphate buffer. The concentration of the sample was 7 μM, and the sample was a month old, stored at 4 °C. Initially fibers were present inside the solution chamber, on heating in superheated water, at around 127 °C the solution turned cloudy, and remained cloudy till 187 °C, theoretically, this solution should eventually clarify. Also, on cooling, the cloudiness disappeared at the same temperature range. Hence this process was reversible, and could be part of the equilibrium curve. For better understanding of this process, a scattering experiment has to be performed. Images of the above process are displayed in the following pages.



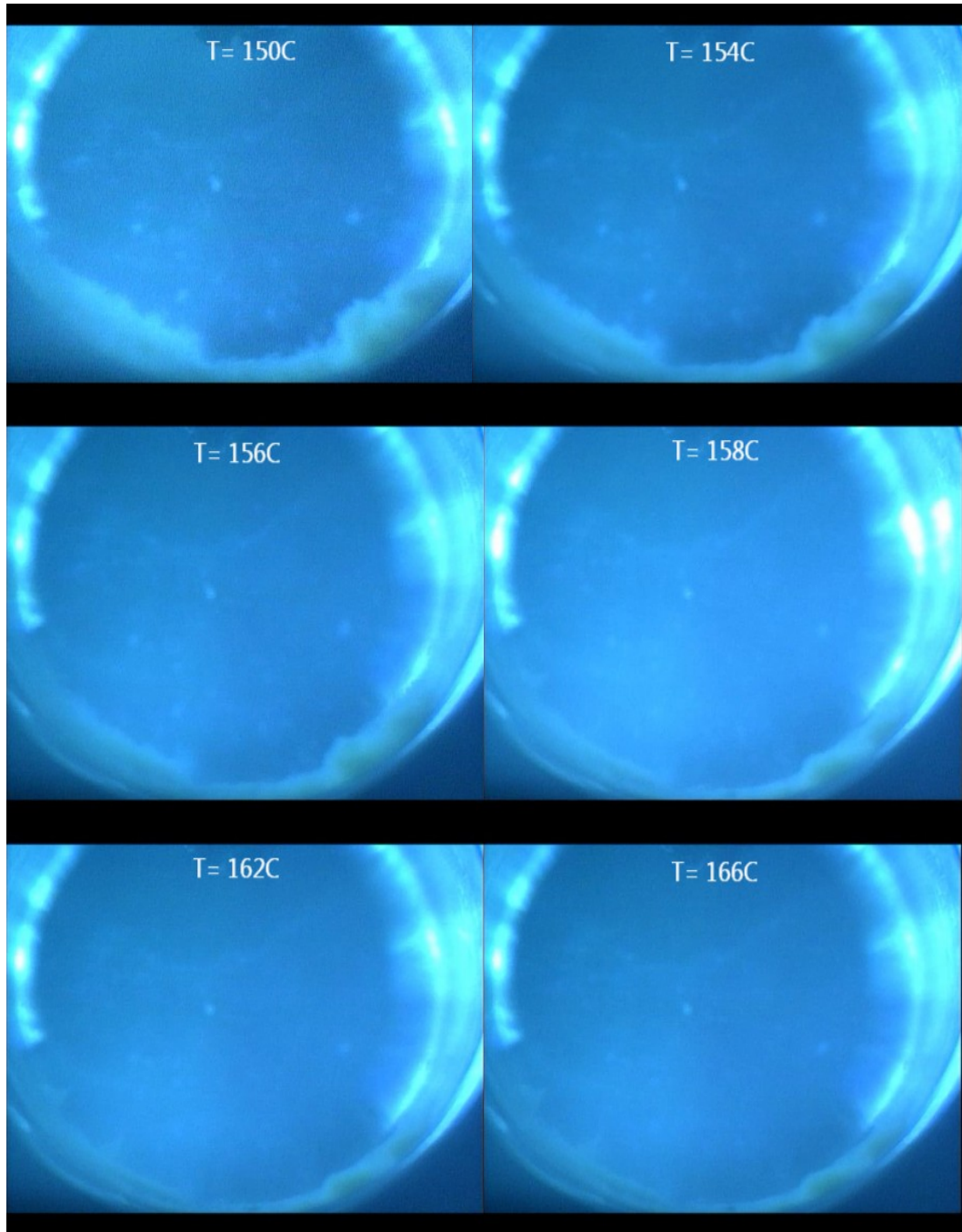


**Figure 3-14. Real time images of heating 1mM polyQ solution.** Real time images for a temperature range of 150 °C to 165 °C

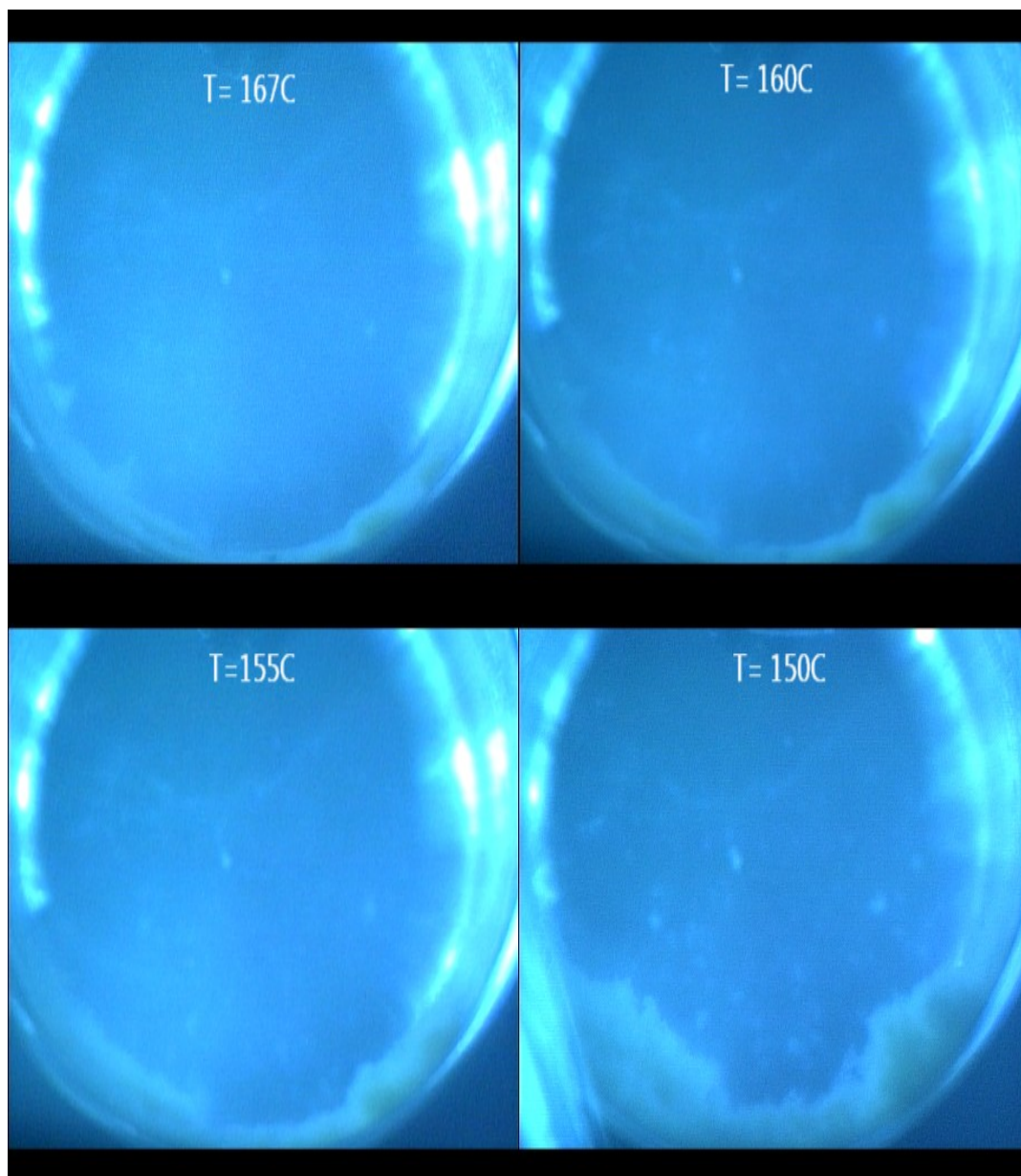


**Figure 3-15. Real time images of cooling 1mM polyQ solution.** Real time images for a temperature range of 165 °C to 150 °C

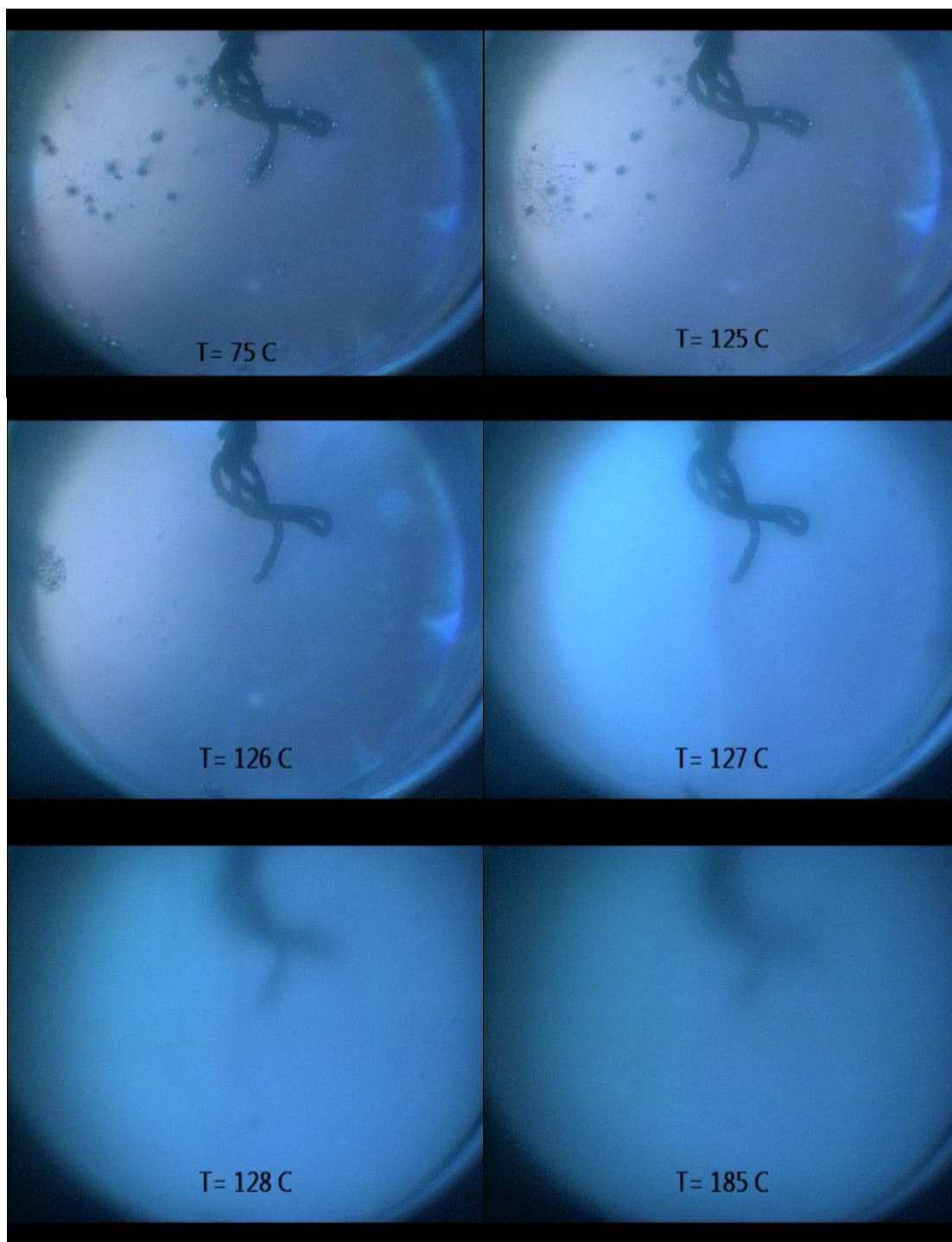


**Figure 3-16. Real time images of heating 7  $\mu$ M CsgA solution.** Real time images for a temperature range of 75  $^{\circ}$ C to 185  $^{\circ}$ C

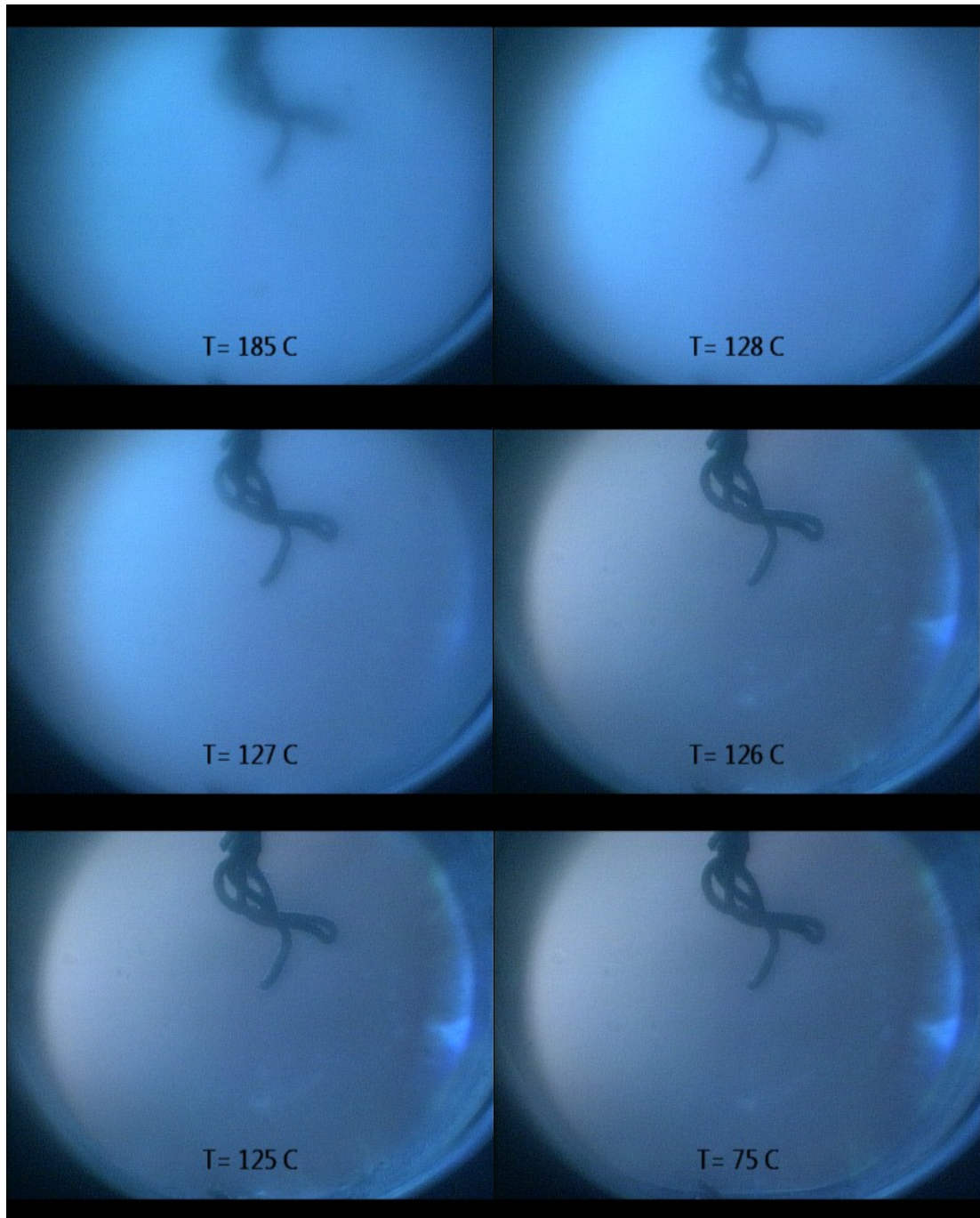


**Figure 3-17. Real time images of cooling 7 μM CsgA solution.** Real time images for a temperature range of 185 °C to 75 °C

# Chapter 4

## Discussion and Conclusions

The above is a report on developing an instrument setup to help quantify polymer-solvent phase transitions and hence gain insights on IDP aggregation processes. We have successfully tested the use of the cell for polymer physics studies. The plot of cloud points of PEG(8000)-water system establishes the use of the device for constructing phase diagrams. Our attempt to study polyglutamine and CsgA aggregation needs further investigation. Integration of the system with a laser setup is required for further analysis, and quantification of the above results on the same.

However, there are three main concerns that still needs to be addressed. Firstly, the heating; we have two heaters on either sides of the cell to ensure uniform heating, but while performing the experiments, we were able to see convection currents, and hence the possibility of unequal heating. This could be solved by better insulation or adding another heater. Also, we could possibly go to higher temperatures by modifying certain parts of the design, like introducing another heater at the bottom of the cell.

Secondly, there is a concern for heat loss to the surrounding air, and hence increasing the power supplied to the system. For our experiments, we were able to cover the whole setup with aluminium foil but there still was a need to supply more power than required to increase the temperature of the system. Hence, further experiments will be carried out in the presence of glass wool or foam. We are going to use better insulation and cover the cell to prevent heat loss to the surroundings for other experiments. After using the cell with protein solutions, the aggregates might stick to the sapphire windows, and this can be cleaned by sonicating the cell with acid inside.

Thirdly, the effect of the rate of heating and cooling. The rate of heating in most of the experiments were much slower than the rate of cooling. Studying the effect of heating in cloud point determination is critical, before experimenting with protein solutions. Also, the effect of quick cooling and slow heating needs to be probed. The above can be done with better insulation, also the use of liquid nitrogen.

Our experiments with polyglutamine solutions(in phosphate buffer) have a positive outcome. We were able to observe a slow and gradual change in the dissolution of the aggregates settled at the bottom i.e. as the temperature is increased beyond 150 °C for 1 mM KKQ(40)KK, the chain-chain interactions start to decrease and there is an increase in chain-solvent interactions. This is consistent with other theories of polymer physics discussed previously. . From the intensity analysis, it is obvious that there is a constant process of aggregate dissolution that is taking place inside the cell. This is the first step to a series of other experiments that can be performed at different concentrations and temperature regimes to construct the phase diagram. However, it is important to integrate the system with a laser to perform small angle light scattering studies to get any insights on the size distribution of the suspended molecules. This can also be used to better quantify the process of disaggregation.

The results obtained using CsgA protein, indicates the formation of another phase. Perhaps the presence of smaller aggregates, however, it is clear that 7 μM CsgA in phosphate buffer does not become monomeric even at 185 °C. Since this process is reversible, we suspect that this process is part of the equilibrium curve and further analysis is required to fully understand the process. Small angle scattering can be easily setup by integrating the current setup with a laser and a pin hole adjustment. This will help us focus light on one spot, and by analyzing the size of the image, and the distance of the camera from the cell, the angle of scattering can be easily determined. Thus a size distribution of the solution can be obtained.

And hence there is a lot of scope for what we can study using this optical cell. The ultimate aim is to completely construct the phase diagram of an IDP, to gain insight on the process of IDP aggregation. After insulating the cell, the homogeneity of heat transfer can be determined by using dyes that change colour with pH. Upon heating the solution, equilibrium of water dissociation shifts towards the right and hence more  $H^+$  ions are released into the environment which decreases the pH of the system. We plan to use 3 dyes: a) bromothymol blue (blue at 7.6 and above and yellow at 6 or below); b) Phenol red (red at 8.2 or above and yellow at 6.8 or below); c) bromocresol purple (purple at 6.8 or above and yellow at 5.2 or below) which change colour with a slight pH change and monitor the path of heat transmission. Hence there exists great potential for future studies with the above described instrument setup.

# Appendix 1

```
%Extract frames from a movie file and analyze overall pixel intensities
%clear all previously stored variables
% p is the intensity
clear movie
clear p
close all

%Make sure you are located in the parent directory of the movie before
%running. Also, be sure to include the .avi extension.
MovieFileName = input('File name:', 's');
%Noise is calculated from a blank movie, i.e. a movie without the
presence of light
Noise =17.8;
%read avi file and get information from the movie
aviinfo(MovieFileName)
movie = aviread(MovieFileName);
% Determine how many frames there are and set the total to zero
NuOfFrames = size(movie, 2);
% Set the extents of the image, based on the size
Rmin = 1;
Rmax = 480;
Rcmin = 1;
Rcmax = 640;
tic;
%initially run this outside since the frame size will not change
for frame=1
% Extract data from each frame of the movie
    thisFrame2=movie(frame).cdata(:, :, 2);
    I (frame)=mean2(thisFrame2);
% Subtract the noise from the frame
    thisFrame=thisFrame2-Noise;
    I2 (frame)=mean2(thisFrame);
% Make a new frame with 0 intensity
    [rows, cols] = size (thisFrame);
    newFrame = zeros(size(thisFrame));
```



```

% Define a condition, add pixels that satisfy the condition into a new
% frame
    for c = Rcmin:Rcmax
        for r = Rrmin:Rrmax
            if thisFrame(r,c) > 0
                newFrame(r,c) = thisFrame(r,c)+Noise;
            end
        end
    end
    end
    p(1)=sum(sum(newFrame))
    imshow(newFrame)
end
% end timer
toc;
% Do the same for all the other frames of the movie
tic;

for frame= 2:NuOfFrames
    thisFrame2=movie(frame).cdata(:,:,2);
    I(frame)=mean2(thisFrame2);
    thisFrame=thisFrame2-Noise;
    I2(frame)=mean2(thisFrame);
    newFrame = zeros(size(thisFrame));
        for c = Rcmin:Rcmax
            for r = Rrmin:Rrmax
                if thisFrame(r,c) > 0
                    newFrame(r,c) = thisFrame(r,c) + Noise;
                end
            end
        end
    end
    p(frame)=sum(sum(newFrame));
end
% Mean Intensity of the movie
Mean=mean2(p)
toc;
% Plot time versus intensity
plot((1:NuOfFrames)/24.97,p)

```

## References

Avallone, E.A., Baumeister, T. (eds.) (1997), *Marks' Standard Handbook for Mechanical Engineers*, 11th ed., McGraw-Hill, Inc. (New York).

Beer, F.P., Johnston, Jr., E.R. (1981), *Mechanics of Materials*, McGraw-Hill, Inc. (New York).

Chiti, F., and Dobson, C. M. (2006) *Protein misfolding, functional amyloid, and human disease*, *Annu Rev Biochem* 75, 333-366.

Christopher James Gregg, Fred P. Stein, Charles K. Morgan, Maciej Radosz (1994); *A variable-volume optical pressure-volume-temperature cell for high-pressure cloud points, densities, and infrared spectra, applicable to superheated fluid solutions of polymers up to 2 kbar*; *Journal of Chemical & Engineering Data* 39(2), 219-224

Crick, S. L., Jayaraman, M., Frieden, C., Wetzel, R., and Pappu, R. V. (2006) *Fluorescence correlation spectroscopy shows that monomeric polyglutamine molecules form collapsed structures in aqueous solutions*, *Proc Natl Acad Sci U S A* 103, 16764-16769

Crick, S. Pappu, R. Thermodynamic and Kinetic Models for Aggregation of Intrinsically Disordered Proteins. *Book chapter in Peptide Folding, Misfolding, and Unfolding*. Ed. Reinhard Schweitzer-Stenner. John Wiley & Sons, Hoboken, NJ. In press.

Dunn, G. and Stachiw, J. (1966.), *Acrylic windows for underwater structures*, *Proc. SPIE*, 7, D-XX-1,

Flory, P. J. (1953) *Principles of Polymer Chemistry*, Cornell University Press, Ithaca and London

Grosberg, A. Y., and Khokhlov, A. R. (1997) *Statistical Physics of Macromolecules (AIP Series in Polymers and Complex Materials)*, 1 ed., AIP Press, New York.

I. Idziak,,D. Avoce,,D. Lessard,,D. Gravel, and,X. X. Zhu(1999); *Thermosensitivity of Aqueous Solutions of Poly(N,N-diethylacrylamide)*; *Macromolecules* 1999 32 (4), 1260-1263

K.B. Doyle, M.A. Kahan(2003), *Design strength of optical glass*, *Optomechanics*, *Proc. SPIE* 5176 .

Lu, J., Carpenter, K., Li, R.-J., Wang, X.-J., and Ching, C.-B. (2004) *Cloud-point temperature and liquid-liquid phase separation of supersaturated lysozyme solution*, *Biophysical Chemistry* 109, 105-112

- Pappu, R. V., Wang, X., Vitalis, A., and Crick, S. L. (2008) *A polymer physics perspective on driving forces and mechanisms for protein aggregation*, Arch Biochem Biophys 469, 132-141
- Pruitt, G. (1986), *Geometric Dimensioning and Tolerancing*, Manufacturing Engineering (July).
- Raos, G., and Allegra, G. (1996) *Chain interactions in poor-solvent polymer solutions: Equilibrium and nonequilibrium aspects*, Macromolecules 29, 6663-6670.
- Raos, G., and Allegra, G. (1996) *Chain collapse and phase separation in poor-solvent polymer solutions: A unified molecular description*, Journal Of Chemical Physics 104, 1626-1645
- Raos, G., and Allegra, G. (1997) *Macromolecular clusters in poor-solvent polymer solutions*, Journal Of Chemical Physics 107, 6479-6490.
- Rubinstein, M., and Colby, R. H. (2003) *Polymer Physics*, Oxford University Press, Oxford and New York
- Sanchez, IC and Stone, MT (2000), *Statistical Thermodynamics of Polymer Solutions and Blends in Polymer Blends Volume 1: Formulation*. Edited by D.R. Paul and C. B. Bucknall, John Wiley & Sons, Inc.
- S. Saiki, N. Kuwahara, M. Nakata and M. Kaneko(1976), *Polymer*,**17**, 685 .
- Szydowski J.,Rebelo L.P.,Van Hook W.A.(1992); *A new apparatus for the detection of phase equilibria in polymer solvent systems by light scattering*; Review of Scientific Instruments, 63 (2), pp. 1717-1725
- Vitalis, A., Wang, X., and Pappu, R. V. (2007) *Quantitative characterization of intrinsic disorder in polyglutamine: insights from analysis based on polymer theories*, Biophys J 93, 1923-1937
- Wang, X., Vitalis, A., Wyczalkowski, M. A., and Pappu, R. V. (2006) *Characterizing the conformational ensemble of monomeric polyglutamine*, Proteins 63, 297-311.
- Y. C. Bae, S. M. Lambert, D. S. Soane, J. M. Prausnitz(1991); *Cloud-point curves of polymer solutions from thermo-optical measurements*; Macromolecules, 24; (15), 4403-4407
- Yan Xiongng (1998); *High-pressure light scattering apparatus to study pressure-induced phase separation in polymer solutions* , Rev. Sci. Instrum. 69, 1463
- Yoder, P.R. (1990), *Opto-Mechanical Systems Design*, 3rdEd., CRC Press, 20

# Vita

## Sai Janani Ganesan

<b>Date of Birth</b>	November 13, 1987
<b>Place of Birth</b>	Pondicherry, India
<b>Degrees</b>	B.E. Biotechnology, July 2009 M.S. Biomedical Engineering, May 2011

May 2011

